## ORIGINAL RESEARCH

# Deficiency of Stomach-Type Claudin-18 in Mice Induces Gastric Tumor Formation Independent of *H pylori* Infection

Koya Suzuki,[1,2,*] Kazuhiro Sentani,[3,*] Hiroo Tanaka,[1,*] Tomoki Yano,[1] Kazuo Suzuki,[4] Masanobu Oshima,[5] Wataru Yasui,[3] Atsushi Tamura,[1] and Sachiko Tsukita[1]

[1]Laboratory of Biological Science, Graduate School of Frontier Biosciences, and Graduate School of Medicine, Osaka University, Osaka, Japan; [2]Research Institute for Diseases of Old Age and Department of Clinical Laboratory Medicine, Graduate School of Medicine, Juntendo University, Tokyo, Japan; [3]Department of Molecular Pathology, Hiroshima University, Institute of Biomedical and Health Sciences, Hiroshima, Japan; [4]Department of Health Protection, Graduate School of Medicine, Asia International Institute of Infectious Disease Control, Teikyo University, Tokyo, Japan; and [5]Division of Genetics, Cancer Research Institute, and Nano Life Science Institute, Kanazawa University, Kanazawa, Japan
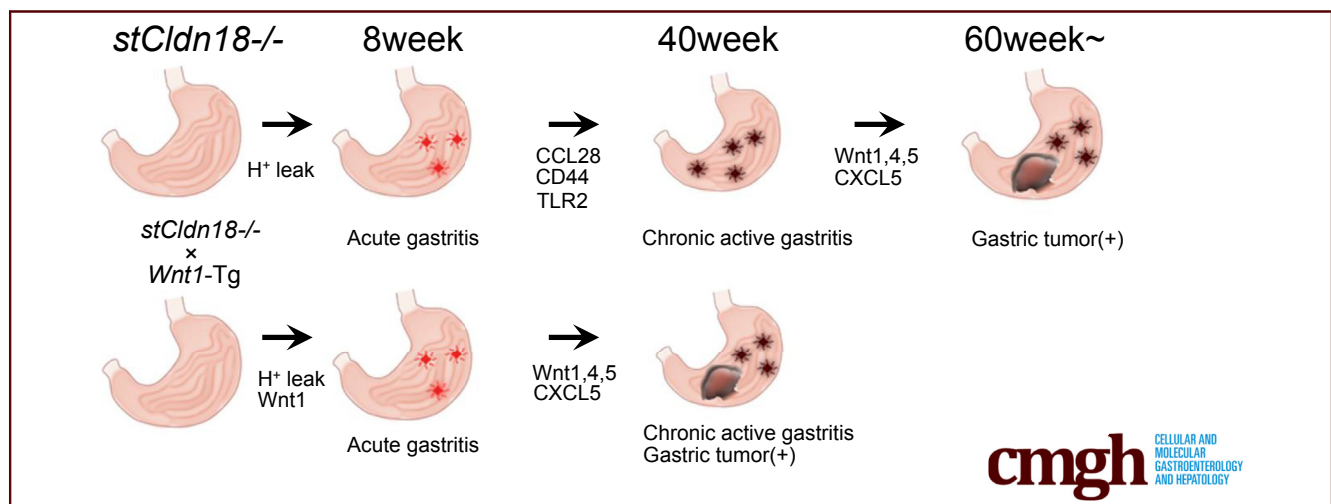
## SUMMARY

Stomach-type claudin-18 (*stCldn18*) deficiency induced gastric tumorigenesis in mice without *H pylori* infection. Several signaling networks, including the cytokine-, stemness-, and Wnt signaling pathways, may be activated under the *stCldn18*-deficiency–induced chronic active gastritis to accelerate the gastric tumorigenesis.

**BACKGROUND & AIMS:** Epithelial cells are joined by tight junctions (TJs) to form a cell sheet. In the stomach, epithelial cell sheet forms an essential barrier against gastric material, including gastric acid. Although the decreased expression of stomach-type claudin-18 (*stCldn18*), a TJ protein, is generally observed in human gastritis and gastric cancer, its pathological roles are not fully understood. We previously reported that mice lacking *stCldn18* (*stCldn18-/-*) exhibit gastric acid leakage through TJs, which induces active gastritis at a young age. Here, we examined the gastric pathologies in mice after long-term *stCldn18* deficiency.

**METHODS:** The gastric pathologies in *stCldn18-/-* mice were sequentially analyzed from youth to old age, and compared to those in humans. To examine the relationship between *stCldn18* deficiency-induced gastric pathologies and Wnt-dependent tumorigenesis, we generated *Wnt1*-over-expressing *stCldn18-/-* mice.

**RESULTS:** *StCldn18-/-* mice developed chronic active gastritis at middle age, with expression of the chemoattractant CCL28. At old age, 20-30% of these mice developed gastric tumors with CXCL5 expression, indicative of EMT. In this process, spasmolytic polypeptide-expressing metaplasia (SPEM) cells appeared. Increased expressions of CD44-variants, TLR2, and CXCL5 indicated age-dependent changes in cell characteristics. Some features of the *stCldn18-/-* mouse gastric tumorigenesis resembled *H pylori*-infection-related human carcinogenesis. The gastric tumorigenesis was accelerated in *Wnt1*-over-expressing *stCldn18-/-* mice, indicating that Wnt is involved in the s*tCldn18-/-* mouse gastric tumorigenesis.

**CONCLUSIONS:** *StCldn18* deficiency induced gastric tumorigenesis in mice without *H pylori* infection. Our findings

revealed that several signaling networks, including the cytokine-, stemness-, and Wnt-signaling pathways, may be activated under the *stCldn18*-deficiency-induced chronic active gastritis to accelerate the gastric tumorigenesis. *(Cell Mol Gastroenterol Hepatol 2019;8:119–142;* https://doi.org/10.1016/j.jcmgh.2019.03.003*)*

*Keywords:* Epithelial Barrier; Tight Junction; Chronic Active Gastritis; SPEM.

---

### See editorial on page 151.

---

Accumulating evidence indicates that the tissue microenvironment plays critical roles in pathophysiological processes including tumor or cancer formation.[1–3] Recent studies suggest that tumor or cancer microenvironments contain immune or nonimmune tumor-related cellular components, extracellular matrix, and interstitial components, which are enclosed by epithelial cell sheets endowed with permselective transcellular and paracellular barrier functions.[4–6] While the epithelial transcellular barrier functions are defined by characteristics of the epithelial cells themselves, such as their plasma membranes and transporters or channels, the paracellular barrier functions are defined by the tight junctions (TJs) between the cells.[7–9]

*Heliobacter pylori* infection is a well-known risk factor for human gastritis and gastric cancer.[10] *H pylori* infects the stomach epithelia and induces gastritis, in which epithelial cell hyperproliferation and dedifferentiation are induced by the CagA-SHP2-MAPK and *Wnt* signaling pathways.[11,12] These signaling pathways are thought to be critical causes of gastric carcinogenesis.[11,12] On the other hand, epithelial cell polarity and the cell-cell adhesion system including TJs are also dysregulated, through the CagA-PAR1 interaction.[13] Thus, a disruption of the TJs' paracellular barrier function, which is thought to cause gastric material including $H^+$ to leak into the submucosal space, might be another important factor contributing to the progression of gastritis and gastric cancer.[14] However, the contribution of the paracellular barrier dysfunction of TJs to gastric pathologies has not been well analyzed.

Claudins (*Cldns*), the 4-transmembrane domain proteins of TJs, are indispensable for TJ formation.[7,15,16] Recent studies revealed that a lack of specific claudins causes inflammation-related pathological conditions.[17–21] These conditions mainly result from aberrant microenvironments generated by the inappropriate passage of water, ions, or small solutes through dysregulated TJs.[8,22,23]

The expression of stomach-type *Cldn18*, a predominant and essential *Cldn* for gastric TJs, is generally decreased in various types of human gastritis and gastric cancer, with or without *H pylori* infection.[14] Recently, a *Cldn18-ARHGAP* fusion gene that disturbs the paracellular barrier function of TJs was also reported in human gastric cancer.[24] Furthermore, we previously reported that stomach-type *Cldn18* gene-knockout (*stCldn18–/–*) mice show acute oxyntic atrophic gastritis at a young age, induced by gastric acid ($H^+$) leakage from the gastric lumen to the submucosal

space through *stCldn18–/–* TJs.[14,25] While it is generally accepted that tumor or cancer microenvironments can be created under chronic inflammatory conditions,[26] it remains unknown whether gastric tumorigenesis or carcinogenesis can also be induced after a long period of *stCldn18*-deficiency–induced gastritis. Consistent with a recent report analyzing *stCldn18–/–* mice, here we independently revealed that gastric tumors developed in aged *stCldn18–/–* mice even without *H pylori* infection.[27] Furthermore, we found that several signaling networks, including the cytokine-, stemness-, and Wnt-signaling pathways, may be activated under the *stCldn18*-deficiency–induced chronic active gastritis to accelerate the gastric tumorigenesis.

## Results

### Induction of Oxyntic Atrophic Gastritis in Young stCldn18–/– Mice and Gastric Tumor Development in Aged stCldn18–/– Mice

To examine the long-term effects of the *stCldn18* deficiency on the gastric pathology, we analyzed *stCldn18–/–* mice at 8, 40, 60, and 100 weeks old (w.o.) (Figure 1*A* and *B*). We previously reported that *stCldn18–/–* mice exhibit oxyntic atrophic gastritis induced by gastric acid leakage from the gastric lumen into the submucosal space at a young age (<8 w.o.).[14] The obvious histological finding in the *stCldn18–/–* mouse stomach was pseudopyloric metaplasia.[14] In this study, we further found that gastric tumors developed in 20%–30% of the *stCldn18–/–* mice at older ages (>60 w.o.) (Figure 1*A* and *B*). As the gastric tumors did not appear in middle-aged *stCldn18–/–* mice (40 w.o.) (Figure 1*A* and *B*), the tumorigenic event might occur between the ages of 40 and 60 w.o.

### Irregular Differentiation and Proliferation of Gastric Epithelial Cells in Young and Aged stCldn18–/– Mice

As gastric hyperplasia developed in the *stCldn18–/–* mice (>40 w.o.) (Figure 1*B*), we examined the age-dependent changes in the differentiation and proliferation of gastric epithelial cells. The number of H,K-ATPase–positive parietal cells was decreased in the *stCldn18–/–* mice at all ages (Figure 2*A*). Ki-67–positive proliferative cells were observed

**Figure 1. Induction of oxyntic atrophic gastritis in young *stCldn18–/–* mice, and gastric tumor development in aged *stCldn18–/–* mice.** (*A*) Macroscopic images of the stomach from *stCldn18+/+* (100 w.o.) and *stCldn18–/–* mice (8, 40, 60, and 100 w.o.). In the old *stCldn18–/–* mice (60, and 100 w.o.), gastric tumors and thick mucus were observed. Representative images from at least 3 independent experiments are shown. Scale bars = 1 cm. (*B*) Hematoxylin and eosin–stained low- and high-magnification images of the stomach from *stCldn18+/+* (100 w.o.) and *stCldn18–/–* mice (8, 40, 60, and 100 w.o.). Lower panels are magnified images of the boxed regions in the upper panels. Representative images from at least 3 independent experiments are shown. Scale bars = 1 mm and 50 μm, respectively.

in the bottom region of the gastric glands in the young *stCldn18–/–* mouse stomach (8 w.o.) (Figure 2*B*). The width of the proliferative zone was increased in the middle-aged *stCldn18–/–* mouse stomach (40 w.o.), and the Ki-67–positive proliferative cells became sparser in the old *stCldn18–/–* mouse stomach (>60 w.o.) (Figure 2*B*). In contrast, the Ki-67–positive proliferative cells were located only in the neck region of the gastric glands in the *stCldn18+/+* mice at all ages (Figure 2*B*). These results suggested that in the *stCldn18–/–* mice, oxyntic atrophic gastritis with abnormal cell differentiation and proliferation occurred at all ages.

## Transition From Active to Chronic Active Gastritis in Middle-Aged stCldn18–/– Mice

It is generally accepted that tumor microenvironments can be created under chronic inflammatory conditions.[26]

In the young *stCldn18–/–* mice (8 w.o.), Gr1-positive neutrophils predominantly infiltrated the stomach (Figure 3*A* and *B*), and only low numbers of CD3+ T lymphocytes were observed (Figure 3*C*), suggesting that acute but not chronic gastritis was present. However, infiltrating CD3+ T lymphocytes were observed in the vicinity of the gastric glands in the stomach of *stCldn18–/–* mice from middle age (>40 w.o.) (Figure 3*C*). Consistent with this result, the number of infiltrating CD4+, and CD8+ T lymphocytes was increased in the stomach of *stCldn18–/–* mice from middle age (>40 w.o.) (Figure 3*D*). Gr1-positive-neutrophils were continuously detected in the stomach of *stCldn18–/–* mice from middle age (>40 w.o.) (Figure 3*A* and *B*), similar to *H pylori* infection–related gastritis.[28] These data indicated that in the *stCldn18–/–* mice, active gastritis transitioned to chronic active gastritis between youth and middle age.
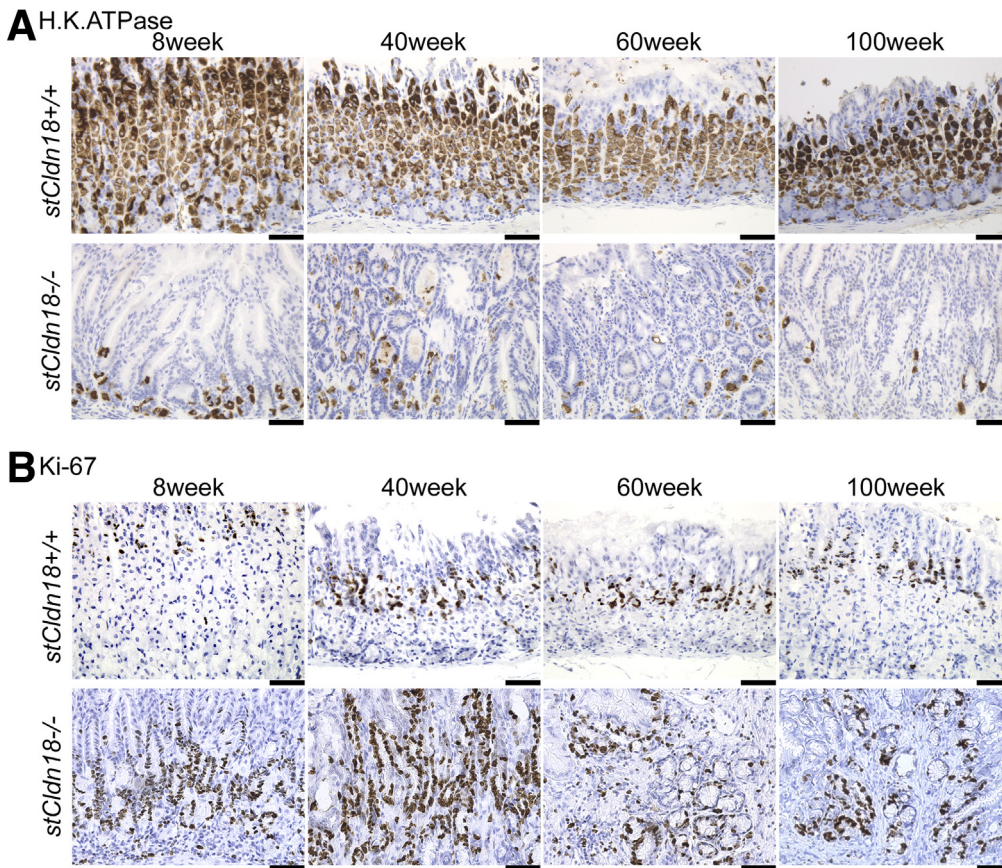
**Figure 2. Irregular differentiation and proliferation of gastric epithelial cells in young and aged stCldn18–/– mice.** (A) Immunohistological micrographs for H,K-ATPase as a parietal cell marker in the stomach from stCldn18+/+ and stCldn18–/– mice (8, 40, 60, and 100 w.o.). The number of parietal cells was decreased in the stCldn18–/– mice at all ages. Representative images from at least 3 independent experiments are shown. Scale bars = 50 $\mu$m. (B) Immunohistological micrographs for Ki-67 as a cell proliferation marker in the stomach from stCldn18+/+ mice and stCldn18–/– mice (8, 40, 60, and 100 w.o.). Representative images from at least 3 independent experiments are shown. Scale bars = 50 $\mu$m.

## Activation of Inflammatory Signaling including CCL28 and CXCL5 in Middle-Aged stCldn18–/– Mice

As active gastritis transitioned to chronic active gastritis in the stCldn18–/– mice with age, we further analyzed the inflammatory signaling associated with the gastritis and the gastric tumorigenesis. The expression levels of general inflammatory cytokines such as interleukin (IL)-1$\beta$, tumor necrosis factor alpha (TNF-$\alpha$), and CXCL1 were upregulated in the stomach of stCldn18–/– mice (Figure 4A).

In H pylori infection–related gastritis and gastric cancer, some cytokines are reported to be related to the disease severity or survival rate.[29–32] Among them, CXCL5, a multifunctional cytokine with neutrophil-attracting, angiogenic, and epithelial-mesenchymal transition (EMT)–inducing activities, is related to the severity of H pylori infection–related human gastric cancer.[33–35] We observed CXCL5-positive gastric epithelial cells in the stCldn18–/– mice from middle age (>40 w.o.) (Figure 4B). Consistent with this finding, the expression level of CXCL5 was significantly increased in the stomach of stCldn18–/– mice at old ages (>60 w.o.) (Figure 4B).

The expression levels of other inflammation-related genes, including STAT3, IKK$\beta$, and NF$\kappa$B, were also upregulated in the stomach of stCldn18–/– mice (Figure 4C). IKK$\beta$/NF-$\kappa$B activation and STAT3 activation are known to have tumorigenic roles, such as in hyperproliferation, antiapoptosis, and angiogenesis.[36–39]

CCL28, a chemokine with a chemoattractant activity for lymphocytes, is upregulated in H pylori infection–related human gastritis, and is of 6 genes that are reported to be significantly correlated with the aggressiveness of gastric cancer.[32,40–43] We observed CCL28-positive cells in the stomach of stCldn18–/– mice from middle age (>40 w.o.) (Figure 4D). The expression level of CCL28 was also increased in the stomach of stCldn18–/– mice, especially at old age (>60 w.o.) (Figure 4D). To further examine CCL28's contribution to the stCldn18–/– mouse gastritis, POL7085, an inhibitor of the CCL28-CCR10 cascade,[44,45] was administered to the stCldn18–/– mice. After 1 week of POL7085 administration, the expression levels of inflammation-related genes such as CXCL5, NF-kB, and IKK$\beta$ were dramatically decreased in the middle-aged stCldn18–/– mice (around 50 w.o.) (Figure 4E). Thus, CCL28 may be a key cytokine for inducing chronic active gastritis in the stCldn18–/– mice.

Collectively, our results showed that CCL28 may be involved in the transition from active gastritis to chronic active gastritis in the stCldn18–/– mice. In addition, the
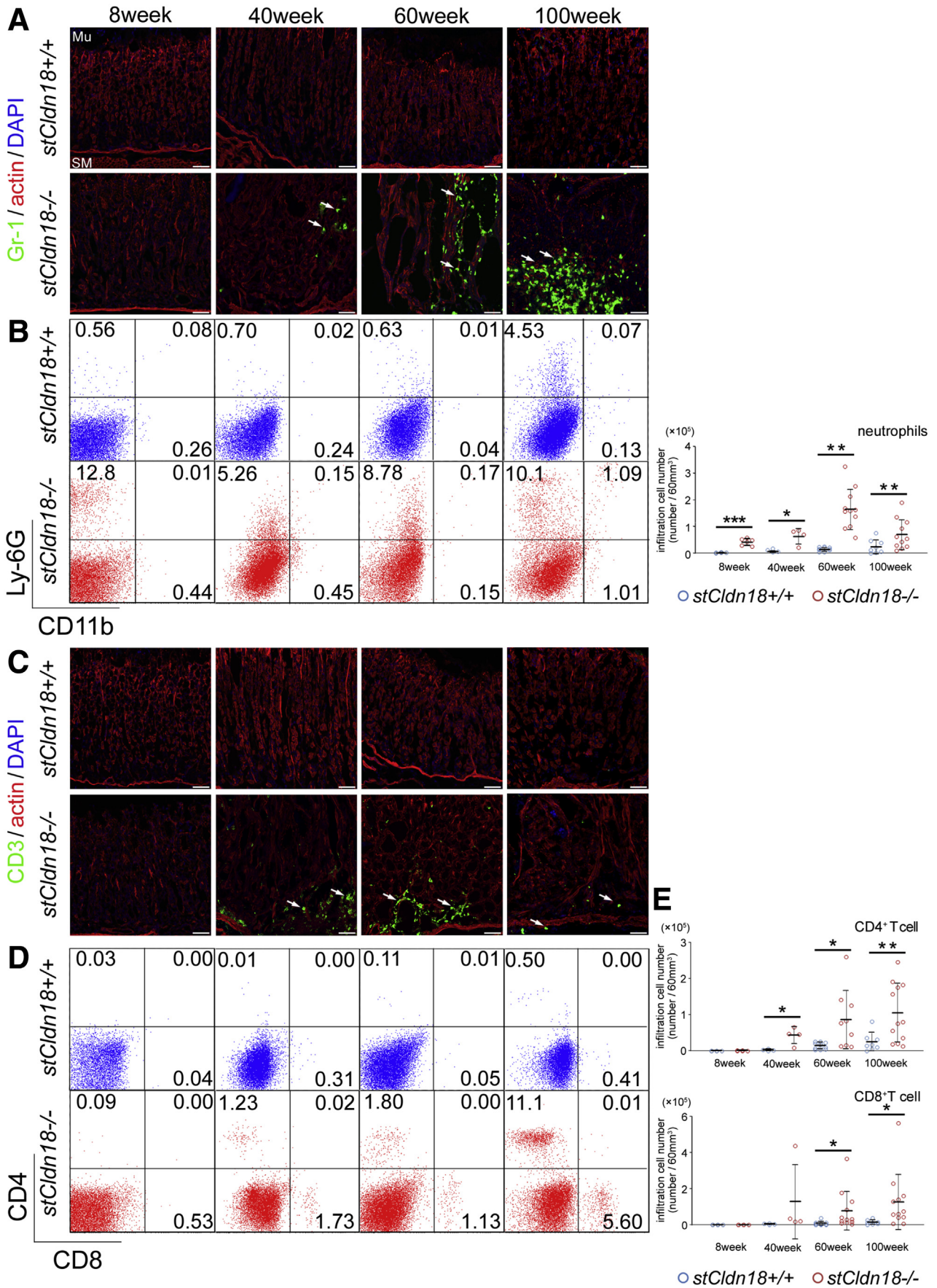
upregulation of other inflammatory signals such as CXCL5, STAT3, and IKK$\beta$/NF-$\kappa$B could be indicative of tumor-directed changes, such as EMT, hyperproliferation, anti-apoptosis, and angiogenesis, in the *stCldn18–/–* mice.

## Induction of Spasmolytic Polypeptide–Expressing Metaplasia in Young and Aged stCldn18–/– Mice

Recently, spasmolytic polypeptide–expressing meta-plasia (SPEM) was suggested to be the origin of cancer stem cells.[6] We previously reported that young *stCldn18–/–* mice exhibit SPEM, which was probably caused by the acute decrease in the number of parietal cells due to gastric acid leakage.[14] In the present study, we found that aged *stCldn18–/–* mice (around 50 w.o.) also showed SPEM, which was double-positive for TFF2 and Pepsin C, near the bottom of the gastric glands (Figure 5A). Ki-67 staining showed that the TFF2 and Pepsin C double-positive SPEM cells were proliferative (Figure 5A).

## Upregulation of CD44 Splicing Variants in Middle-Aged stCldn18–/– Mice

SPEM cells are known to express splicing variants of CD44, which are often found at high expression levels in cancer stem cells.[46–49] In this respect, conventional real-time polymerase chain reaction (RT-PCR) showed that the CD44 v8-v10 variants were highly expressed in the stomach of *stCldn18–/–* mice from middle age (>40 w.o.) (Figure 5B), and CD44-positive SPEM cells were observed in the stomach of aged *stCldn18–/–* mice (Figure 5C). These results suggested that the tumor-directed stemness of the SPEM cells increased in the *stCldn18–/–* mice. Supporting this hypothesis, the expression level of TLR2, an innate immune receptor with a role in maintaining stemness,[50] increased in the *stCldn18–/–* mice with age (Figure 6A). We also found CD44 and TLR2 double-positive cells in the stomach of *stCldn18–/–* mice (Figure 6B). In addition, the expression levels of other stemness markers such as SOX2, c-Myc, Ascl2, and matrix metalloproteinase-7 (MMP7) were increased in the stomach of the aged *stCldn18–/–* mice (Figure 6C).[51] The expression level of MMP7 was especially increased in the stomach of *stCldn18–/–* mice at 100 w.o., which is notable because MMP7 is known to be involved in cell invasion and in the stemness of cancer stem cells.[51]

## Development of Intestinal Metaplasia and Ectopic Gastric Glands in Aged stCldn18–/– Mice
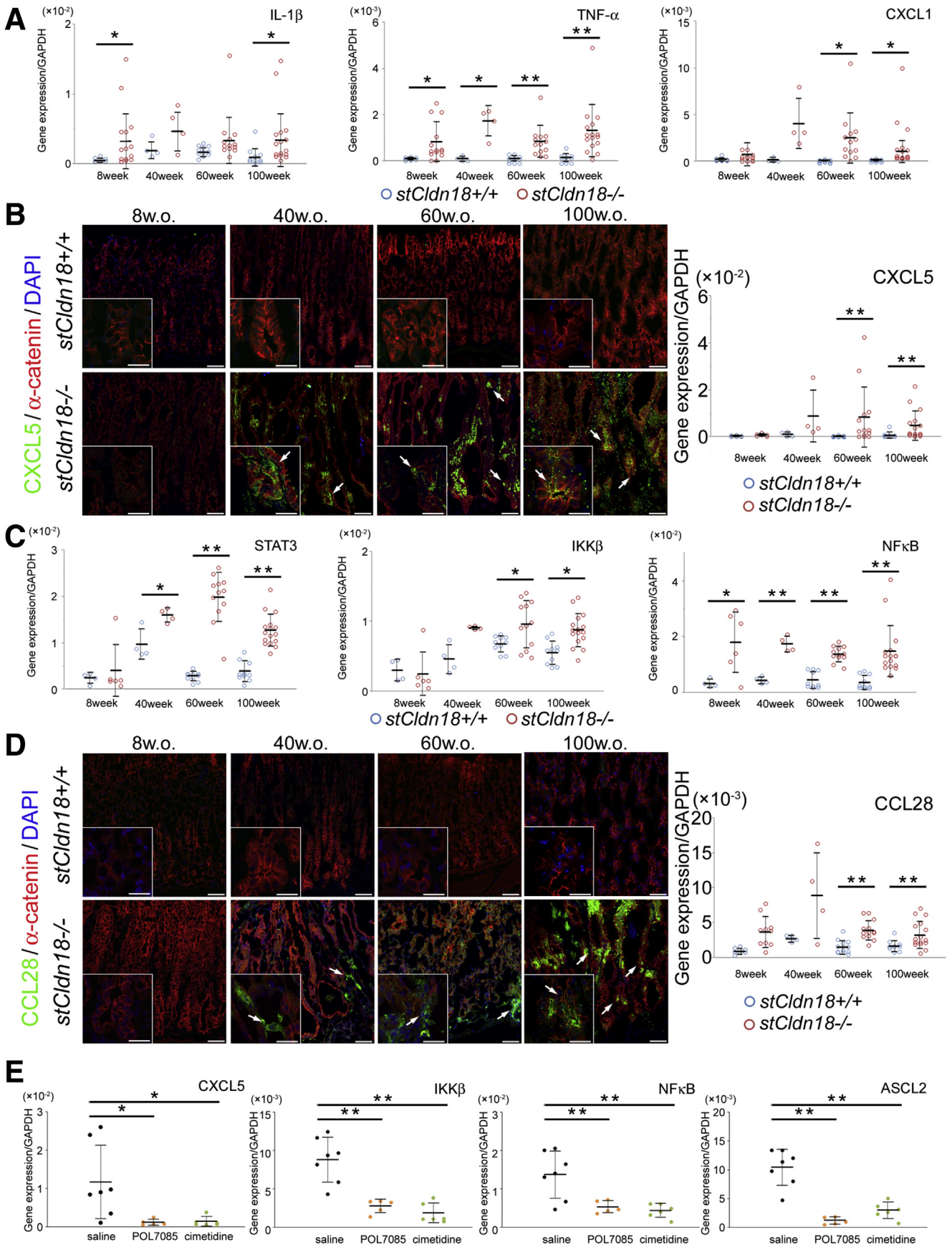
Gastric intestinal metaplasia is known to be a precancerous change in which the gastric mucosa is replaced by intestinal epithelium.[52] In this respect, the expression levels of *Cldn2*, *Cldn4*, and *Cldn7* were significantly increased in the stomach of *stCldn18–/–* mice (Figure 7A), and these *Cldns* are known to be highly expressed in intestinal epithelial cells.[53] Consistent with this finding, *Cldn2*- or *Cldn7*-positive cells were clearly observed in the stomach of *stCldn18–/–* mice (Figure 7B). Furthermore, villin, a marker for intestinal epithelial cells, was detected in the stomach of *stCldn18–/–* mice (Figure 7B). These results suggested that gastric intestinal metaplasia developed in the *stCldn18–/–* mice. Importantly, the changes in the expression levels of these *Cldns* could also be associated with the gastric pathologies of the *stCldn18–/–* mice.

In the old *stCldn18–/–* mice (100 w.o.), ectopic gastric glands formed outside the gastric mucosa (Figure 7C). This ectopic gastric gland was histologically similar to the "gastritis cystica profunda" or to the "invasive submucosal gland," which are observed in *H pylori*–related gastritis,[54] and it was recently reported that the "invasive submucosal gland" represents the stage between intestinal metaplasia and gastric cancer in a study in Mongolian gerbils.[55] Although the ectopic gastric gland we observed had features of intestinal epithelium, which is villin-, *Cldn2*-, *Cldn4*-, or *Cldn7*-positive (Figure 7E), in addition to being CD44- or Ki-67–positive (Figure 7D), it did not show any obvious dysplastic changes such as nuclear atypia.

## Activation of Wnt Signaling in Aged stCldn18–/– Mice

*Wnt* signaling is known to be activated in 30%–50% of human gastric cancers.[56] Considering that CXCL5, CD44, and MMP7, which were upregulated in the aged *stCldn18–/–* mouse stomach, are related to be *Wnt* signaling,[57–59] *Wnt*

**Figure 3.** (*See previous page*). **Transition from active to chronic active gastritis in middle-aged *stCldn18–/–* mice.** (*A*) Immunofluorescence micrographs for Gr-1 (*green*) as a neutrophil marker co-stained with actin (*red*) and DAPI (*blue*) in the stomach from *stCldn18+/+* and *stCldn18–/–* mice (8, 40, 60, and 100 w.o.). Gr-1–positive neutrophils (*arrows*) were clearly observed in the *stCldn18–/–* mice. Representative images from at least 3 independent experiments are shown. Scale bars = 50 $\mu$m. (*B*) (*Left*) Fluorescence-activated cell sorting (FACS) data for Ly-6G–positive neutrophils in the stomach from *stCldn18+/+* (*top*) and *stCldn18–/–* (*bottom*) mice (8, 40, 60, and 100 w.o.) (n = 8/group). The number of Ly-6G–positive neutrophils was increased in the *stCldn18–/–* mice at all ages (8, 40, 60, and 100 w.o.). (*Right*) Results are expressed as mean ± SD. Comparisons between 2 groups were performed using Student's *t* test, and differences with $P < .05$ were considered statistically significant. *$P < .05$; **$P < .01$; ***$P < .001$. (*C*) Immunofluorescence micrographs for CD3 as a lymphocyte marker co-stained with actin (*red*) and DAPI (*blue*) in the stomach from *stCldn18+/+* mice and *stCldn18–/–* mice (8, 40, 60, and 100 w.o.). CD3-positive T lymphocytes (*arrows*) were clearly observed in the stomach of *stCldn18–/–* mice only after middle-age (40, 60, and 100 w.o.). Representative images from at least 3 independent experiments are shown. Scale bars = 50 $\mu$m. (*D*) Fluorescence-activated cell sorting (FACS) data for CD4-positive and CD8-positive T lymphocytes in the stomach from *stCldn18+/+* (*top*) and *stCldn18–/–* (*bottom*) mice (8, 40, 60, and 100 w.o.) (n = 8/group). The numbers of CD4-positive and CD8-positive T lymphocytes were increased in the *stCldn18–/–* mice only after middle-age (40, 60, 100 w.o.). (*E*) Results are expressed as mean ± SD. Comparisons between 2 groups were performed using Student's *t* test, and differences with $P < .05$ were considered statistically significant. *$P < .05$; **$P < .01$.

**A**
IL-1β, TNF-α, CXCL1 gene expression/GAPDH plots across 8week, 40week, 60week, 100week for *stCldn18+/+* and *stCldn18-/-*.

**B**
CXCL5 / α-catenin / DAPI immunofluorescence images (8w.o., 40w.o., 60w.o., 100w.o.) for *stCldn18+/+* and *stCldn18-/-*; CXCL5 gene expression/GAPDH plot.

**C**
STAT3, IKKβ, NFκB gene expression/GAPDH plots across 8week, 40week, 60week, 100week for *stCldn18+/+* and *stCldn18-/-*.

**D**
CCL28 / α-catenin / DAPI immunofluorescence images (8w.o., 40w.o., 60w.o., 100w.o.) for *stCldn18+/+* and *stCldn18-/-*; CCL28 gene expression/GAPDH plot.

**E**
CXCL5, IKKβ, NFκB, ASCL2 gene expression/GAPDH plots for saline, POL7085, cimetidine.

signaling might be involved in the *stCldn18–/–* mouse gastric tumorigenesis. In this respect, the nuclear localization of $\beta$-catenin, a marker for *Wnt* signaling activation,[60] was observed in the stomach of *stCldn18–/–* mice from middle age (>40 w.o.) (Figure 8*A*). Furthermore, the expression level of *Wnt1a* was especially increased in the stomachs with gastric tumors of 100-w.o. *stCldn18–/–* mice (Figure 8*B*). The expression levels of *Wnt4* and *Wnt5* gradually increased in the stomach of *stCldn18–/–* mice with age (Figure 8*C*). These results showed that Wnt signaling was increasingly activated in the stomach of *stCldn18–/–* mice with age. Thus, the activation of *Wnt* signaling could be related to the gastric tumorigenesis in *stCldn18–/–* mice.

## *Acceleration of Gastric Tumorigenesis Under Chronic Active Gastritis in* Wnt1-*Overexpressing Transgenic* stCldn18–/– *Double-Mutant Mice*

As previously reported, *Wnt1*-overexpressing transgenic (*Wnt1*-Tg) mice developed small gastric polyps without severe gastritis.[61] To examine the relationship between *stCldn18*-deficiency–induced chronic gastritis and *Wnt*-dependent gastric tumorigenesis, we crossed *Wnt1*-Tg with *stCldn18–/–* mice to obtain double-mutant (DM) mice. The *Wnt1*-Tg and DM mice were born, and grew with a macroscopically normal appearance, similar to the *stCldn18–/–* mice.

At a young age (8 w.o.), the *Wnt1*-Tg mice showed no severe gastric pathologies, in contrast to the *stCldn18–/–* and DM mice (Figure 9*A–C*). The DM mouse stomach also showed increased expression levels of inflammatory cytokines such as IL-1$\beta$, TNF-$\alpha$, CXCL1, and CCL28, similar to the *stCldn18–/–* mouse stomach (Figure 9*B*). A few CD3$^+$ T lymphocytes were

observed in the DM mouse stomach (Figure 9*C*). These results indicated that at the young age (8 w.o.), the DM mice developed gastritis similarly to the *stCldn18–/–* mice.

At middle age (40 w.o.), all of the DM mice developed gastric tumors, while none of the *stCldn18–/–* mice did (Figure 10*A*). Hematoxylin and eosin–stained images of the DM mouse stomach showed that the density of the gastric glands was increased in a back-to-back manner (Figure 10*B*), suggesting that dysplastic changes were induced. Inflammatory cytokines such as IL-1$\beta$, TNF-$\alpha$, CXCL1, CCL28, and CXCL5 were upregulated in both the *stCldn18–/–* and DM mouse stomachs (Figure 10*C*). The number of CD3$^+$ T lymphocytes was also increased in the *stCldn18–/–* and the DM mouse stomach compared with the *stCldn18+/+* mouse and *Wnt1*-Tg mouse stomach (Figure 10*D*). At this age, the *Wnt1*-Tg mice did not show severe gastritis/gastric tumor formation but small foveolar hyperplasia, the phenotype of which was reported previously (Figure 10*A–D*).[61]

Collectively, the extent of gastritis in the DM mice was similar to that in the *stCldn18–/–* mice, except for the level of CXCL5, which is a target of *Wnt* signaling. (Figure 10*A–D*). These findings suggested that the *Wnt*-dependent gastric tumorigenesis might be accelerated under the severe gastritis induced by the *stCldn18* deficiency.

## *Similarity of Gastric Tumorigenesis in* stCldn18–/– *Mice to* H pylori *Infection–Related Tumorigenesis in Humans*

To compare the mouse model and human disease, we analyzed the expression levels of *Cldn18* in human gastritis

**Figure 4.** (*See previous page*). **Activation of inflammatory signals including CCL28 and CXCL5 in aged *stCldn18–/–* mice.** (*A*) Expression levels of IL-1$\beta$, TNF-$\alpha$, and CXCL1 in the stomach from *stCldn18+/+* (n = 8, 4, 11, 10) and *stCldn18–/–* mice (n = 14, 4, 13, 16) (8, 40, 60, and 100 w.o.) quantified by qRT-PCR. Gene expressions were normalized to glyceraldehyde-3-phosphate dehydrogenase (GAPDH). Results are expressed as mean ± SD. Comparisons between 2 groups were performed using Student's *t* test, and differences with *P* < .05 were considered statistically significant. \**P* < .05; \*\**P* < .01. (*B*) Immunofluorescence micrographs for CXCL5 (*green*) co-stained with $\alpha$-catenin (*red*) and DAPI (*blue*) in the stomach from *stCldn18+/+* mice and *stCldn18–/–* mice (8, 40, 60, and 100 w.o.). CXCL5 signals were clearly observed in the stomach of *stCldn18–/–* mice after middle-age (40, 60, and 100 w.o.) (*arrows*). High-magnification images are shown in insets. Representative images from at least 3 independent experiments are shown. Scale bars = low magnification: 50 $\mu$m, high magnification: 10 $\mu$m. (*Right*) Expression level of CXCL5 in the stomach from *stCldn18+/+* (n = 8, 4, 12, 10) and *stCldn18–/–* mice (n = 6, 4, 13 16) (8, 40, 60, and 100 w.o.) quantified by qRT-PCR. Gene expressions were normalized to GAPDH. Results are expressed as mean ± SD. Comparisons between 2 groups were performed using Student's *t* test, and differences with *P* < .05 were considered statistically significant. \*\**P* < .01. (*C*) Expression levels of STAT3, IKK$\beta$, and NF-$\kappa$B in the stomach from *stCldn18+/+* (n = 4, 4, 10, 10) and *stCldn18–/–* mice (n = 6, 4, 12, 16) (8, 40, 60, and 100 w.o.) quantified by qRT-PCR. Gene expressions were normalized to GAPDH. Results are expressed as mean ± SD. Comparisons between 2 groups were performed using Student's *t* test, and differences with *P* < .05 were considered statistically significant. \**P* < .05; \*\**P* < .01. (*D*) (*Left*) Immunofluorescence micrographs for CCL28 (*green*), a lymphocyte chemoattractant and maintainer of chronic inflammation, co-stained with $\alpha$-catenin (*red*) and DAPI (*blue*) in the stomach from *stCldn18+/+* and *stCldn18–/–* mice (10, 40, 60, and 100 w.o.). CCL28 signals were clearly observed in the stomach of the *stCldn18–/–* mice after middle-age (40, 60, and 100 w.o.) (*arrows*). High-magnification images are shown in insets. Representative images from at least 3 independent experiments are shown. Scale bars = low magnification: 50 $\mu$m, high magnification: 10 $\mu$m. (*Right*) Expression level of CCL28 in the stomach from *stCldn18+/+* (n = 8, 4, 12, 10) and *stCldn18–/–* (n = 10, 4, 13 16) mice (8, 40, 60, and 100 w.o.) quantified by qRT-PCR. Gene expressions were normalized to GAPDH. Results are expressed as mean ± SD. Comparisons between 2 groups were performed using Student's *t* test, and differences with *P* < .05 were considered statistically significant. \*\**P* < .01. (*E*) Expression levels of CXCL5, IKK$\beta$, NF$\kappa$B, and ASCL2 in the stomach from *stCldn18+/+* and *stCldn18–/–* mice (around 50 w.o.) after POL7085 or cimetidine treatment, quantified by qRT-PCR (n: *stCldn18–/–* = 7, 5, 6, given saline, POL7085, and cimetidine, respectively). Gene expressions were normalized to GAPDH. Results are expressed as mean ± SD. Comparisons between 2 groups were performed using Student's *t* test, and differences with *P* < .05 were considered statistically significant. \**P* < .05; \*\**P* < .01.

**A**



**B**



**C**
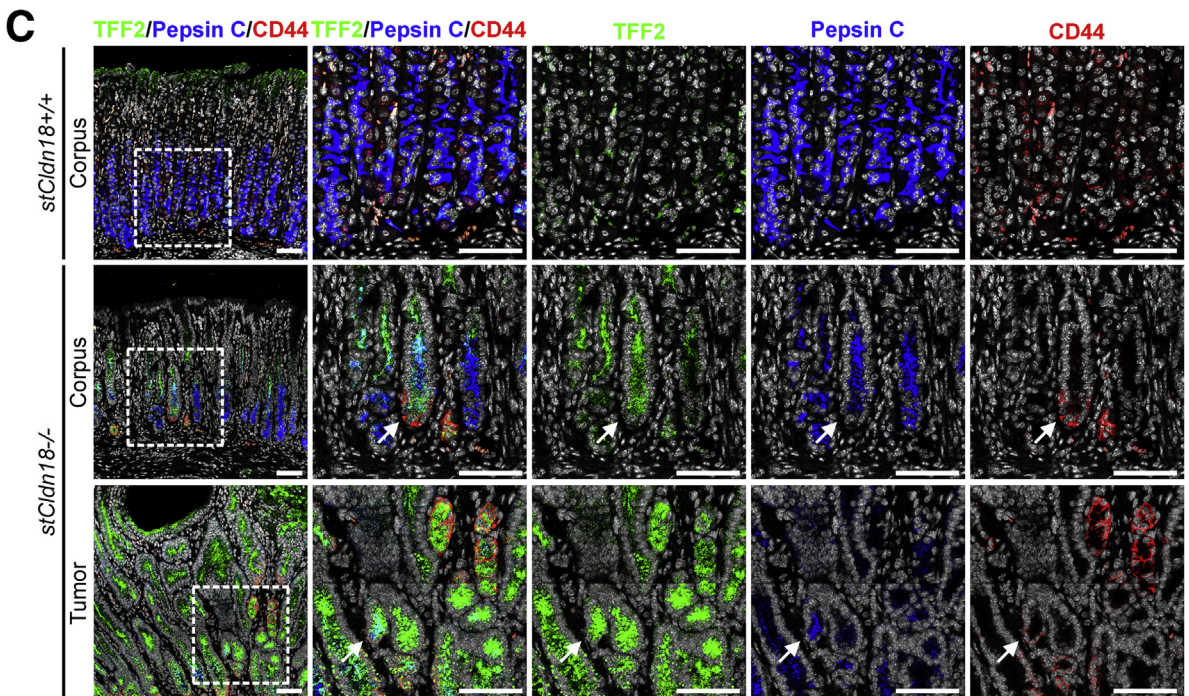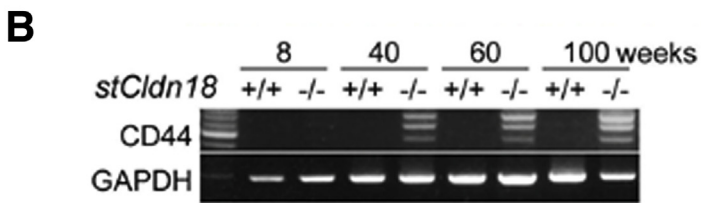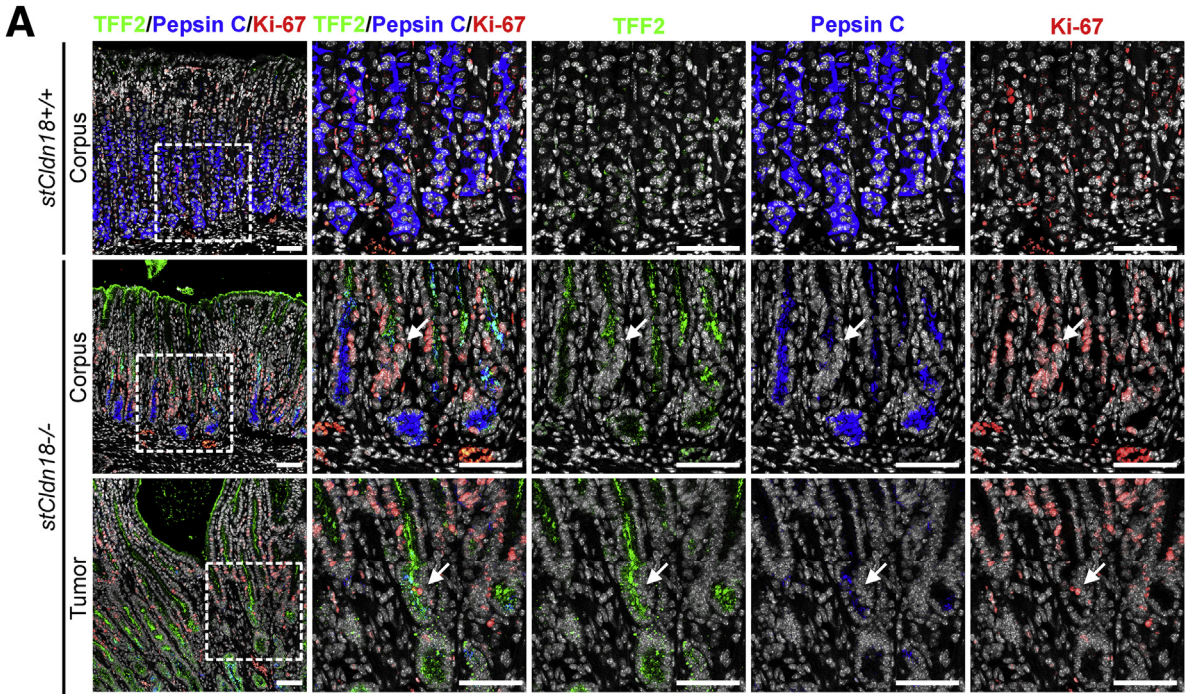
samples and in various human gastric tumors. Gastric hyperplastic polyp (HP), which is usually associated with *H pylori* infection in humans, develops in the context of chronic inflammation.[62] Fundic gland polyp (FGP), a major human tumor, is a hyperplasia that is not associated with either inflammation or *H pylori* infection, and is considered to be different from the inflammation-related process such as that seen in the *stCldn18–/–* mice.[63] Another disease, Peutz-Jeghers polyp (PJP), is an autosomal-dominant inherited disorder characterized by hamartoma in the digestive tract, including gastric tumors, and also has a different disease process from that seen in the *stCldn18–/–* mice.[64]

Pathologically, the tumor regions in the *stCldn18–/–* mice closely resembled human HP (Figure 11*A*). The expression level of *Cldn18* in HP was clearly lower than that in FGP or PJP (Figure 11*B*), and the expression level of CXCL5 in HP was clearly higher than that in FGP or PJP (Figure 11*C*). These results suggested that the expression level of *Cldn18* was inversely correlated with that of CXCL5 in HP. These data suggested that the *stCldn18–/–* mouse gastric tumors at least partly resembled human HP.

Furthermore, we noted that the *Cldn18* expression level in a gastric adenocarcinoma that originated from HP was reduced (Figure 11*D*). The CXCL5 expression were also upregulated in the adenocarcinoma region of the human stomach (Figure 11*D*).

## Toxic Effects of Gastric Acid in Aged stCldn18–/– Mice

In the *stCldn18–/–* mice, the long-term gastritis continued without healing. In this respect, only a few parietal cells remained in the aged *stCldn18–/–* mice, suggesting that gastric acid secreted by these cells promoted the gastritis. After 1 week of administering the $H_2$-blocker cimetidine, an inhibitor of gastric acid secretion, to middle-aged *stCldn18–/–* mice (around 50 w.o.), the expression levels of inflammation-related genes such as CXCL5, IKK$\beta$, and NF-kB were dramatically decreased (Figure 4*E*). This result suggested that the remaining parietal cells could still secrete gastric acid to promote gastritis.

Importantly, it was still unclear to what extent the gastric acid leakage due to the *stCldn18* deficiency directly contributed to the gastritis and gastric tumorigenesis. Our present findings suggested that the activation of several signaling pathways, including the cytokine-, stemness-, and Wnt-signaling pathways, might contribute to these gastric

pathologies under the severe gastritis induced by the *stCldn18* deficiency. For example, the administration of cimetidine or POL7085 dramatically inhibited the gastritis, and also decreased the expression level of Ascl2, a stemness marker, in middle-aged *stCldn18–/–* mice (around 50 w.o.) (Figure 4*E*). Thus, it was possible that the stemness was also increased under the chronic gastritis induced by the *stCldn18* deficiency.

## Process of Gastric Tumorigenesis in Young to Aged stCldn18–/– Mice Without H pylori Infection

Based on our findings, we propose a scheme in which the loss of *stCldn18* creates a microenvironment that leads to chronic active gastritis and gastric tumor formation in the absence of *H pylori* infection (Figure 12). The active gastritis, which occurred in young *stCldn18–/–* mice (<8 w.o.), transitioned to chronic active gastritis with expression of the chemoattractant CCL28 in middle-aged *stCldn18–/–* mice (40 w.o.). In the old *stCldn18–/–* mice (>60 w.o.), gastric tumors formed with the expression of CXCL5, which promoted EMT downstream of *Wnt*. In this tumorigenesis process, SPEM cells appeared. Changes in cell characteristics were suggested by the upregulation of CD44, TLR2, and *Wnt*. Furthermore, the gastric tumorigenesis was accelerated in *Wnt1*-Tg *stCldn18–/–* DM mice.

Our analysis provides evidence that long-term *stCldn18* deficiency induces chronic active gastritis and then gastric tumors in mice even in the absence of *H pylori* infection. Several signaling pathways, including the cytokine-, stemness-, and Wnt-signaling pathways, may be activated to accelerate the gastric tumorigenesis under the *stCldn18* deficiency–induced chronic active gastritis. Notably, the process of *stCldn18–/–* mouse gastric tumorigenesis partially resembled that of *H pylori* infection–related human carcinogenesis.

## Discussion

Disruption of the paracellular barrier function of TJs is thought to be an important factor in the progression of gastritis and gastric cancer,[14] although its contribution to gastric pathologies has not been thoroughly analyzed. In this respect, we previously reported that in young *stCldn18–/–* mice, acute oxyntic atrophic gastritis is induced by the leakage of gastric acid from the gastric lumen to the submucosal space through *stCldn18–/–* TJs. In the present study,

**Figure 5.** (*See previous page*). **Induction of spasmolytic polypeptide–expressing metaplasia (SPEM) in young and aged *stCldn18–/–* mice.** (*A*) Immunofluorescence micrographs for TFF2 (*green*) and Pepsin C (*blue*) as SPEM cell markers co-stained with Ki-67 (*red*) and DAPI (*white*) in the stomach from *stCldn18+/+* and *stCldn18–/–* mice (around 50 w.o.). Right panels are magnified images of the boxed regions in the left panels. SPEM cells were clearly observed in the stomach of the *stCldn18–/–* mice. The Ki-67 signals partially coincided with the SPEM cells (*arrows*). Representative images from at least 2 independent experiments are shown. Scale bars = 100 $\mu$m. (*B*) Expression levels of the tumor-related alternatively spliced variants of CD44, and GAPDH in the stomach from *stCldn18+/+* and *stCldn18–/–* mice (8, 40, 60, and 100 w.o.) quantified by conventional RT-PCR. (*C*) Immunofluorescence micrographs for TFF2 (*green*) and Pepsin C (*blue*) as SPEM cell markers co-stained with CD44 (*red*) and DAPI (*white*) in the stomach from *stCldn18+/+* and *stCldn18–/–* mice (around 50 w.o.). Right panels are magnified images of the boxed regions in the left panels. CD44-positive cells were clearly observed in the stomach of the *stCldn18–/–* mice. The CD44 signals partially coincided with the SPEM cells (*arrows*). Representative images from at least 3 independent experiments are shown. Scale bars = 100 $\mu$m.

**A**



**B**



**C**
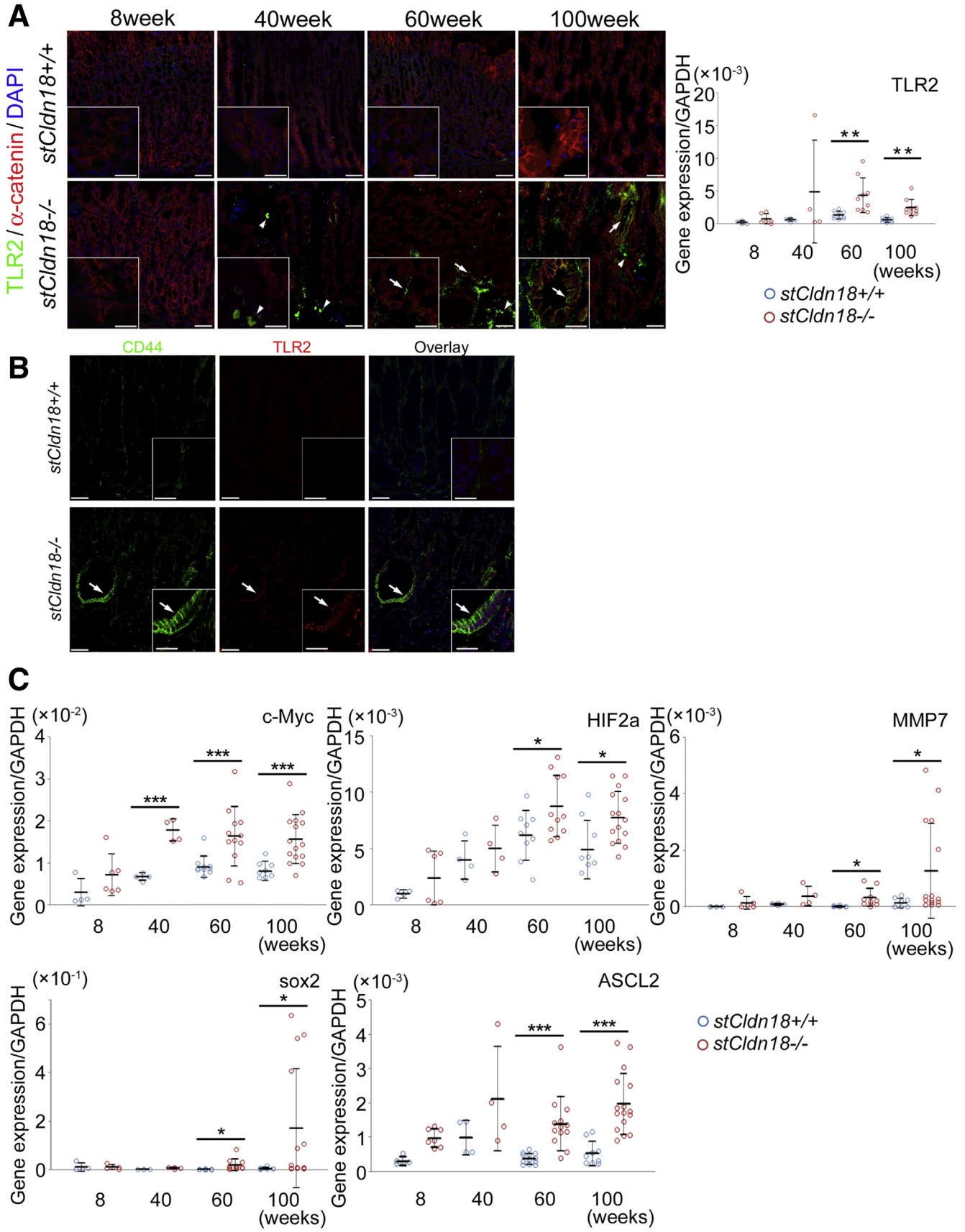
we analyzed the *stCldn18–/–* mice over their entire lifetime. Our analysis provides evidence that long-term *stCldn18* deficiency induces gastric tumors to form under chronic active gastritis in mice without *H pylori* infection, in a process involving several signaling pathways, including the cytokine-, stemness-, and Wnt-signaling–activated pathways.

CCL28 could be a key chemokine causing the *stCldn18–/–* mouse gastritis to become chronic, based on the following findings. The expression of CCL28 is reported to be induced by hypoxia-inducible factors under hypoxic conditions,[42] suggesting that hyperproliferative tumor-related hypoxia could upregulate CCL28 expression in the *stCldn18–/–* mice (Figure 6C). It is also reported that the expression of CD44 v8-v10 variants is induced by hypoxia to promote cell proliferation.[65] Thus, a positive feedback loop involving CD44 upregulation, cell proliferation, and hypoxia could increase the CCL28 expression to accelerate the transition from active to chronic active gastritis in the *stCldn18–/–* mice.

Recently, SPEM cells were suggested to be the origin of cancer stem cells.[66] Evidence also suggests that prolonged gastritis eventually changes the stemness of SPEM cells.[67] In the *stCldn18–/–* mice, the expression levels of stemness markers were increased from middle age, when chronic active gastritis was induced. Therefore, we speculate that the *stCldn18* deficiency–induced chronic active gastritis promoted tumor-directed changes in the SPEM cells.

The EMT upregulates cell migration and invasion in cancer development.[68] In this respect, we observed that CXCL5, a downstream target of *Wnt* signaling and an EMT-inducible cytokine, was increased during the *stCldn18–/–* mouse gastric tumorigenesis. Although invasive gastric cancer did not form in the *stCldn18–/–* mice, EMT presumably caused some morphological changes in the gastric glands to accelerate the tumorigenesis.

The expression of CXCL5, a target of *Wnt* signaling, was dramatically increased in the DM mice at middle age (40 w.o.). However, the CXCL5 expression was not increased in DM mice at a young age (8 w.o.), when severe gastritis was not observed. These findings suggested that the chronic active gastritis induced by *stCldn18* deficiency dramatically potentiated the effect of *Wnt* signaling. Consistent with this possibility, the CXCL5 expression was upregulated in

*stCldn18–/–* mice especially at old age. Thus, changes in the characteristics of the *stCldn18*-deficiency–induced gastritis might be required for the activation of *Wnt* signaling to accelerate the gastric tumorigenesis. As *Wnt* signaling is reported to be coordinated with Notch to regulate gastric stem cell proliferation and differentiation, it is possible that the upregulation of Notch is also involved in the *stCldn18–/–* mouse gastric tumorigenesis.[69]

Fox's group recently reported that gastric pathologies including gastritis and gastric tumors were observed in their *Cldn18–/–* mice, similar to our *stCldn18–/–* mice.[27] They globally analyzed the signaling pathways by RNA sequencing, and, like us, found that *Wnt* signaling was involved in the *Cldn18–/–* mouse gastric tumorigenesis.[27] In our study, we further used DM mice to examine the tumorigenic roles of *Wnt* signaling under the chronic gastritis induced by *stCldn18* deficiency.

It was recently reported that in lung-type *Cldn18* gene knockout (*luCldn18–/–*) mice, *luCldn18* loss induced the nuclear localization of YAP, which promoted the development of lung adenocarcinoma.[70] Although the *luCldn18* expression that was upregulated in the stomach of our *stCldn18–/–* mice,[14] the nuclear localization of YAP could might be related to the gastric tumorigenesis in our *stCldn18–/–* mice.

Collectively, we found that the *stCldn18* deficiency induced the development of gastric tumors under chronic active gastritis in the absence of *H pylori* infection. Age-dependent changes in several signaling networks involving inflammation-, stemness-, and *Wnt*-related pathways, may accelerate this gastric tumorigenesis in a multi-faceted manner.

# Materials and Methods
## Ethics Statement

Animal experiments were performed in accordance with protocols approved by the Animal Studies Committee of Osaka University School of Medicine. Recombinant DNA experiments were carried out in accordance with protocols approved by Osaka University. Studies using human samples were performed at Hiroshima University in accordance with protocols approved by the Hiroshima University School of Medicine Ethics Committee.

---

**Figure 6.** (*See previous page*). **Upregulation of TLR2 in aged *stCldn18–/–* mice.** (A) (*Left*) Immunofluorescence micrographs for TLR2 (*green*) co-stained with $\alpha$-catenin (*red*) and DAPI (*blue*) in the stomach from *stCldn18+/+* and *stCldn18–/–* mice (8, 40, 60, and 100 w.o.). High-magnification images are shown in insets. TLR2-positive cells were clearly observed in the stomach of *stCldn18–/–* mice after middle age (40, 60, and 100 w.o.). At middle age (40 w.o.), the TLR2-positive cells did not show the characteristics of gastric epithelium (*arrowheads*), but at old age (60, and 100 w.o.), the TLR2-positive cells might have been gastric epithelial cells (*arrows*). Representative images from at least 2 independent experiments are shown. Scale bars = low magnification: 50 $\mu$m, high magnification: 50 $\mu$m. (*Right*) Expression level of TLR2 in the stomach from *stCldn18+/+* (n = 4, 4, 10, 10) and *stCldn18–/–* mice (n = 8, 4, 12, 16) (8, 40, 60, and 100 w.o.) quantified by qRT-PCR. Results are expressed as mean ± SD. Comparisons between 2 groups were performed using Student's *t* test, and differences with $P < .05$ were considered statistically significant. **$P < .01$. (B) Immunofluorescence micrographs for CD44 (*green*), co-stained with TLR2 (*red*) in the stomach from *stCldn18+/+* and *stCldn18–/–* mice (100 w.o.). High-magnification images are shown in insets. CD44-and TLR2-double-positive cells were clearly observed in the stomach of the *stCldn18–/–* mice (*arrows*). Representative images from at least 3 independent experiments are shown. Scale bars = low magnification: 50 $\mu$m, high magnification: 50 $\mu$m. (C) Expression levels of c-Myc, hypoxia-inducible factor HIF2a, MMP7, SOX2, and ASCL2 in the stomach from *stCldn18+/+* (n = 5, 4, 12, 9) and *stCldn18–/–* (n = 9, 4, 13, 16) mice (8, 40, 60, and 100 w.o.) quantified by qRT-PCR. The expression level of MMP7 was especially increased in the stomach of the 100 w.o. *stCldn18–/–* mice. Gene expressions were normalized to GAPDH. Results are expressed as mean ± SD. Comparisons between 2 groups were performed using Student's *t* test, and differences with $P < .05$ were considered statistically significant. *$P < .05$; ***$P < .001$.
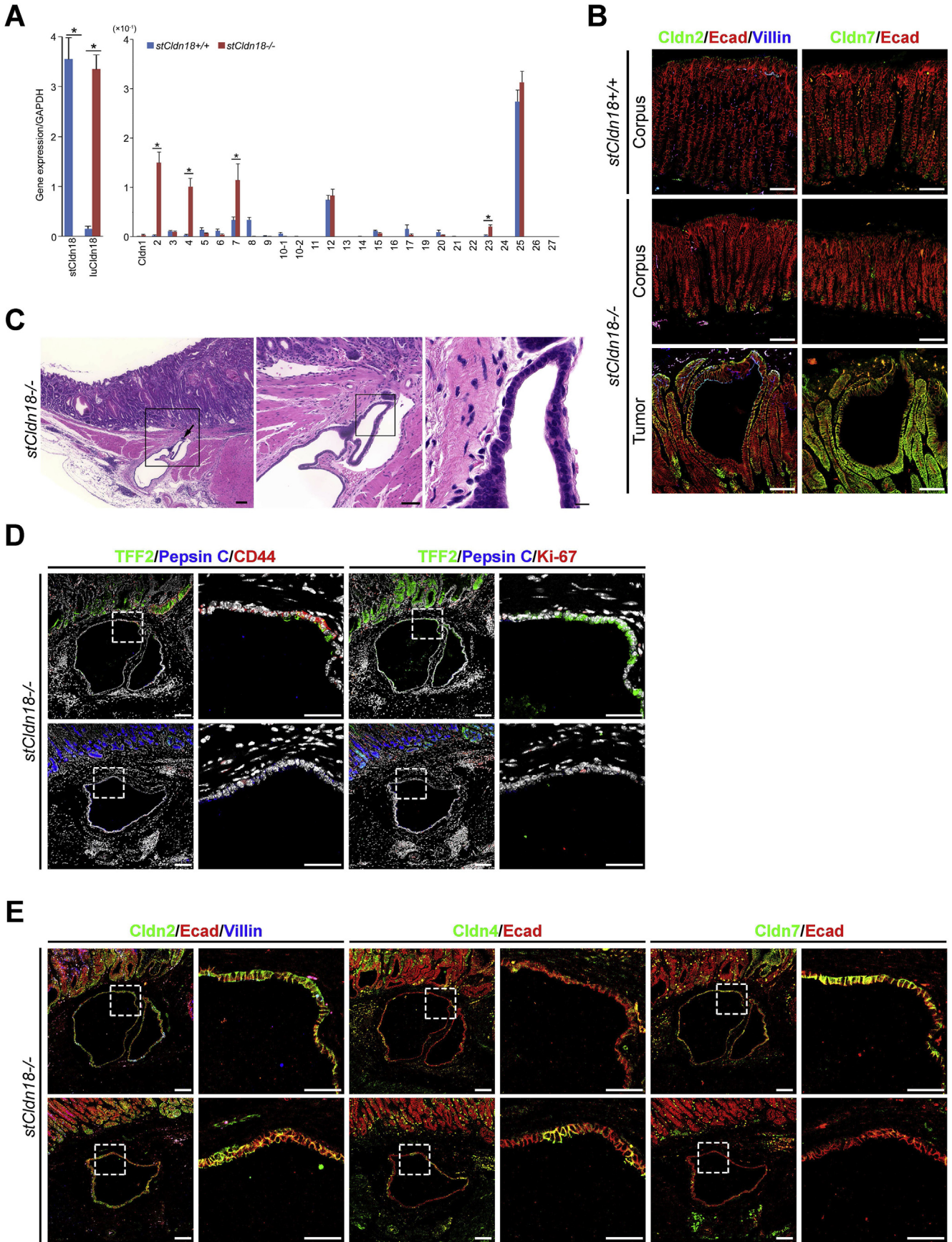
### Antibodies

Antibodies used for immunochemical staining and fluorescence-activated cell sorting (FACS) analyses are listed in Table 1.

### Generation of stCldn18–/–, Wnt1-*Tg, and* Wnt1-*Tg* stCldn18–/– DM Mice

The method for generating *stCldn18*-deficient (*stCldn18*–/–) mice was previously reported.[14] In brief, the first exon of the mouse *stCldn18* locus was replaced with a neomycin-resistance gene by a conventional homologous recombination technique. The obtained heterogeneous, A129 R1 ES cells were injected into ICR blastocysts, and transplanted into the ovaries of foster mother mice. The high-percentage male chimeras were bred with female C57BL/6J mice, and the resulting heterogeneous mice were intercrossed to generate *stCldn18*–/– mice.

The method for generating *Wnt1*-Tg mice was previously reported.[61] Briefly, *Wnt1* complementary DNA was excised and cloned into pBluescript (Stratagene, La Jolla, CA) to construct a pK19-*Wnt1* transgenic vector. The transgenic vector was microinjected into fertilized eggs of F1 (C3H and C57BL/6) hybrid females, which were crossed with C57BL/6 males to generate *Wnt1*-Tg mice. *Wnt1* transgene expression driven under keratin 19 (K19) promotor is transcriptionally active in the gastric epithelium.[61]

*stCldn18*–/– and *Wnt1*-Tg mice were intercrossed to generate *Wnt1*-Tg *stCldn18*–/– DM mice.

Mice were bred in specific pathogen-free conditions, and were negative for *H pylori*.

### Histological Staining

For the immunohistological staining of paraffin sections, a freshly excised mouse stomach was fixed with 10% neutral buffered formalin solution at 4°C for 24 hours. After fixation, the stomach was dehydrated in a graded ethanol series and embedded in paraffin using a Spin Tissue Processor (Thermo Scientific, Tokyo, Japan). The samples in paraffin were cut into 5-$\mu$m-thick sections, deparaffinized twice by immersion in xylene at room temperature for 3 minutes, and hydrated by being passed through a series of decreasing ethanol concentrations (100%, 95%, 90%, 80%, 70%, and 50%) at room temperature for 1 minute each. The samples were then blocked with phosphate-buffered saline (PBS) containing 1% bovine serum albumin at room temperature for 10 minutes, and stained with primary antibodies at 4°C overnight. After 3 washes with PBS, the samples were stained with Horseradish peroxidase (HRP)-labeled secondary antibodies for 1 hour at room temperature. After 3 washes with PBS, the samples were developed with 3,3'-Diaminobenzidine tetrahydrochloride (DAB) at room temperature for 10 minutes. The samples were then rinsed with running tap water for 5 minutes. After counterstaining with hematoxylin, the samples were dehydrated, and mounted with Marinol (Muto Pure Chemicals Co, Ltd, Tokyo, Japan; Cat. No. 20091).

For the immunofluorescence staining of frozen sections, the mouse stomach was washed with ice-cold PBS, embedded in Tissue-Tek O.C.T. Compound (Sakura Finetek Japan Co, Ltd, Tokyo, Japan; Cat. No. 4583), and was frozen in liquid $N_2$. The frozen samples were cut into 5-$\mu$m-thick sections, and air dried at room temperature for 20 minutes. The sections were fixed with methanol at –20°C for 10 minutes, or with PBS containing 2% paraformaldehyde at room temperature for 10 minutes after permeabilization with PBS containing 0.1% Triton-X100 at room temperature for 10 minutes. The samples were then blocked with PBS containing 1% bovine serum albumin at room temperature for 10 minutes. After blocking, the samples were stained with primary antibody overnight at 4°C. After 3 washes with PBS, the samples were stained with fluorescently labeled secondary antibodies and with 1 mg/mL 4′,6-diamidino-2-phenylindole (DAPI) for 1 hour at room temperature. After 3 washes with PBS and 1 with deionized distilled water, the samples were embedded in fluorescence mounting medium (Dako Japan, Tokyo, Japan; Cat. No. S3023).

**Figure 7. (*See previous page*). Development of intestinal metaplasia and ectopic gastric gland in aged *stCldn18*–/– mice.** (*A*) Expression levels of *Cldns* in the stomach from st*Cldn18*+/+ (n = 6), and *stCldn18*–/– (n = 7), mice at 100 w.o. quantified by qRT-PCR. The expression levels of *Cldn2*, *4*, *7*, and *luCldn18* were significantly increased in the stomach of *stCldn18*–/– mice at old age. Gene expressions were normalized to GAPDH. Results are expressed as mean ± SD. Comparisons between 2 groups were performed using Student's *t* test, and differences with *P* < .05 were considered statistically significant. n.s., not significant. *\*P* < .05. (*B*) Immunofluorescence micrographs for Cldn2 or Cldn7 (*green*) co-stained with E-cadherin (*red*) and with or without villin (*blue*) in the stomach from *stCldn18*+/+ and *stCldn18*–/– mice (around 50 w.o.). Representative images from at least 3 independent experiments are shown. Scale bars = 100 $\mu$m. (*C*) Hematoxylin and eosin–stained images of the ectopic gastric gland in aged *stCldn18*–/– mice. Ectopic gastric glands were found in 1 of 3 old *stCldn18*–/– mice by examining stomach tissue slices. Right panels are magnified images of the boxed regions in the left panels. Representative images from at least 2 independent experiments are shown. Scale bars = 100, 50, 10 $\mu$m, left to right panel. (*D*) (*Left*) Immunofluorescence micrographs for TFF2 (*green*) and Pepsin C (*blue*) as SPEM cell markers co-stained with CD44 (red) and DAPI (*white*) in the ectopic gastric gland from *stCldn18*–/– mice (around 50 w.o.). (*Right*) Representative immunofluorescence micrographs for TFF2 (*green*), and Pepsin C (*blue*) as SPEM cell markers co-stained with Ki-67 (*red*) and DAPI (*white*) in the ectopic gastric gland from *stCldn18*–/– mice (around 50 w.o.). *Right* panels are magnified images of the boxed regions in the left panels. Representative images from at least 2 independent experiments are shown. Scale bars = 100, 50 $\mu$m, left to right panel. (*E*) (*Left*) Immunofluorescence micrographs for *Cldn2* (*green*) co-stained for E-cadherin (*red*) and villin (*blue*) in the ectopic gastric gland from *stCldn18*–/– mice (around 50 w.o.). Right panels are magnified images of the boxed regions in the left panels. Representative images from at least 2 independent experiments are shown. Scale bars = 100, 50 $\mu$m, left to right panel. (*Middle, Right*) Immunofluorescence micrographs for *Cldn4* or *Cldn7* (*green*) co-stained for E-cadherin (*red*) in the ectopic gastric gland from *stCldn18*–/– mice (around 50 w.o.). Right panels are magnified images of the boxed regions in the left panels. Representative images from at least 2 independent experiments are shown. Scale bars = 100, 50 $\mu$m, left to right panel.
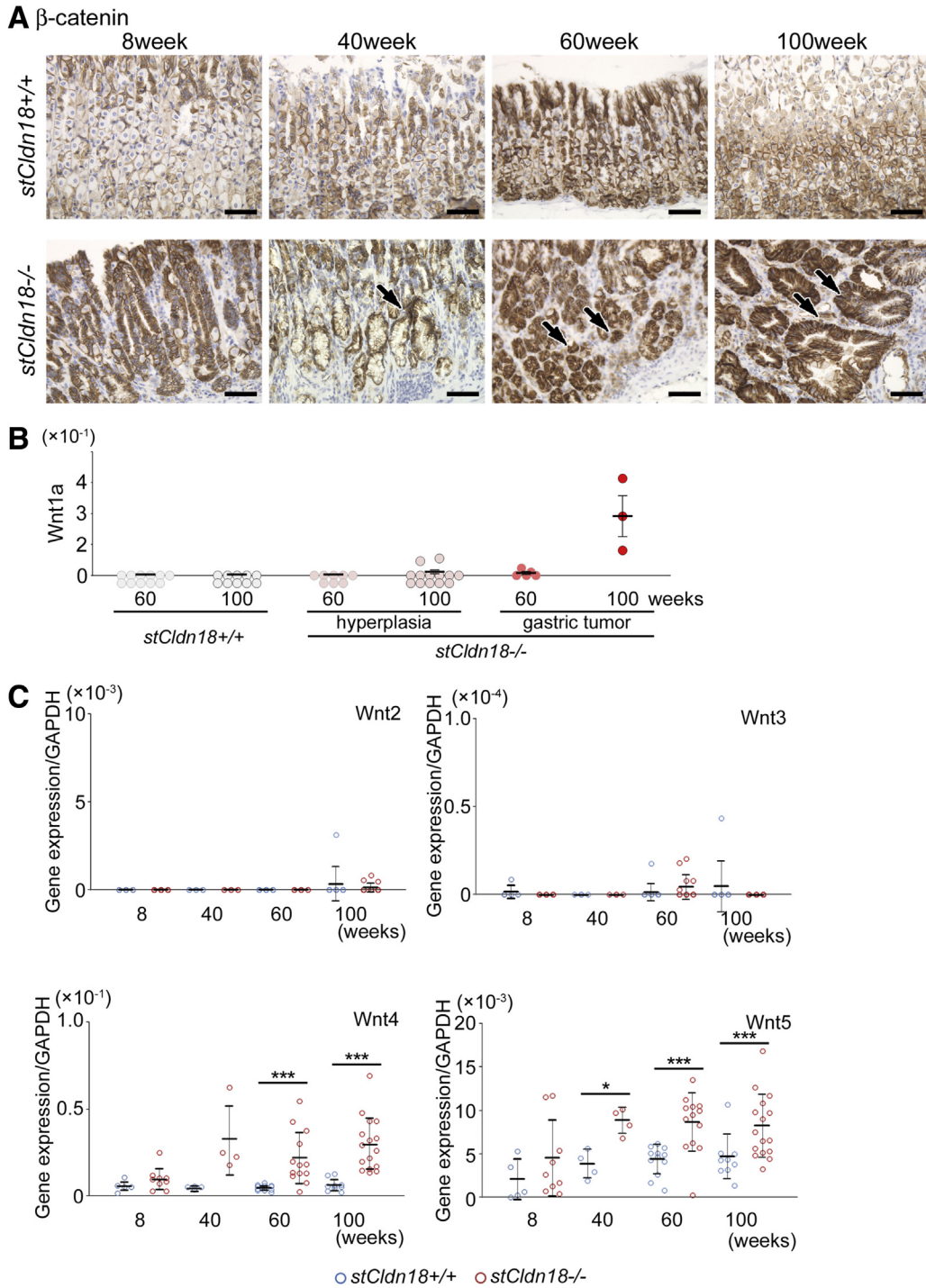
**Figure 8. Activation of *Wnt* signaling in aged *stCldn18–/–* mice.** (*A*) Immunohistological micrographs for $\beta$-catenin as an EMT marker in the stomach from *stCldn18+/+* and *stCldn18–/–* mice (8, 40, 60, and 100 w.o.). A nuclear localization of $\beta$-catenin, indicative of *Wnt* signaling activation, was observed in the stomach of *stCldn18–/–* mice after middle age (40, 60, and 100 w.o.) (*arrows*). Representative images from at least 3 independent experiments are shown. Scale bars = 50 $\mu$m. (*B*) Expression level of *Wnt1a* in the stomach from stCldn18+/+ mice (n = 11, 10), and stCldn18–/– mice with hyperplasia (n = 8, 13), with gastric tumor (n = 5, 3) (60, and 100 w.o.) quantified by qRT-PCR. *Wnt1a* was especially increased in the gastric tumors of the 100-w.o. *stCldn18–/–* mice. Gene expressions were normalized to GAPDH. (*C*) Expression level of *Wnt2*, *Wnt3*, *Wnt4*, and *Wnt5* in the stomach from *stCldn18+/+* (n = 5, 4, 12, 9) and *stCldn18–/–* (n = 9, 4, 13, 16) mice (10, 40, 60, and 100 w.o.), quantified by qRT-PCR. Gene expressions were normalized to GAPDH. Results are expressed as mean $\pm$ SD. Comparisons between 2 groups were performed using Student's *t* test, and differences with $P < .05$ were considered statistically significant. *$P < .05$; ***$P < .001$.
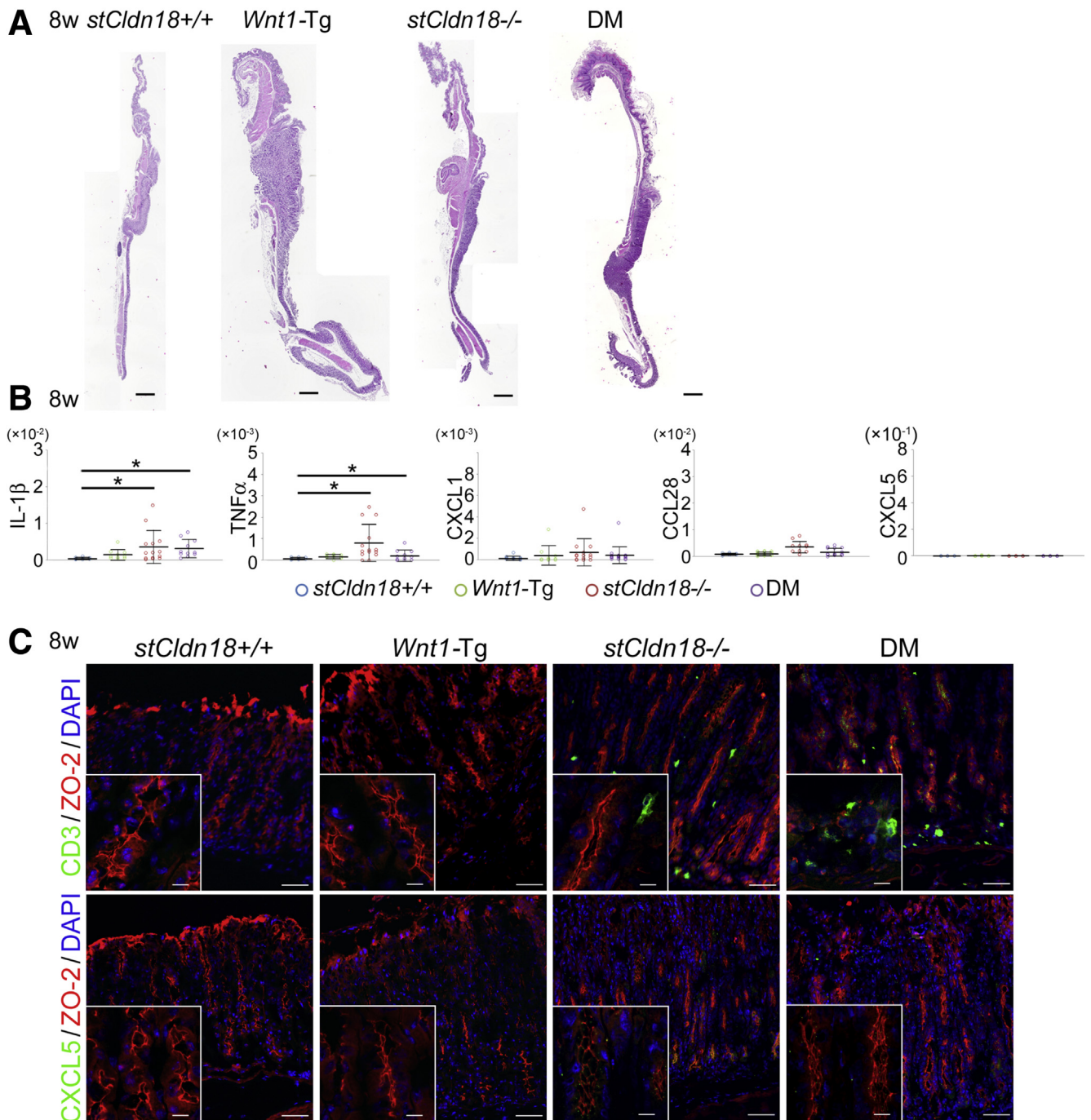
**Figure 9. No tumor formation in young Wnt1-Tg stCldn18–/– DM mice.** (A) Hematoxylin and eosin–stained images of the stomach from stCldn18+/+, Wnt1-Tg, stCldn18–/–, and Wnt1-Tg mice crossed with stCldn18–/– DM mice at a young age (8 w.o.). No obvious difference was detected in the stomachs between stCldn18–/– and DM mice at the young age. Representative images from at least 3 independent experiments are shown. Scale bars = 1 mm. (B) Expression levels of IL-1$\beta$, TNF-$\alpha$, CXCL1, CCL28, and CXCL5 in the stomach from stCldn18+/+, Wnt1-Tg, stCldn18–/–, and DM mice at a young age (8 w.o.) quantified by qRT-PCR (n = 8, 4, 10, 11). No significant differences were detected between the stomachs of stCldn18–/– and DM mice at the young age. Gene expressions were normalized to GAPDH. Results are expressed as mean ± SD. Comparisons among more than 3 groups were performed using the Kruskal-Wallis 1-way analysis of variance on ranks ($P < .01$) followed by the Steel-Dwass test. *$P < .05$. (C) Immunofluorescence micrographs for CD3 or CXCL5 (green) co-stained with ZO-2 (red) and DAPI (blue) in the stomach from stCldn18+/+, Wnt1-Tg, stCldn18–/–, and DM mice at a young age (8 w.o.). High-magnification images are shown in insets. No significant differences were detected between the stomachs of stCldn18–/– and DM mice at the young age. Representative images from at least 3 independent experiments are shown. Scale bars = low magnification: 100$\mu$m, high magnification: 10 $\mu$m.

**A** 40w     *stCldn18+/+*     *Wnt1*-Tg     *stCldn18-/-*     DM

**B** 40w

**C** 40w

○ *stCldn18+/+*    ○ *Wnt1*-Tg    ○ *stCldn18-/-*    ○ DM

**D** 40w     *stCldn18+/+*     *Wnt1*-Tg     *stCldn18-/-*     DM
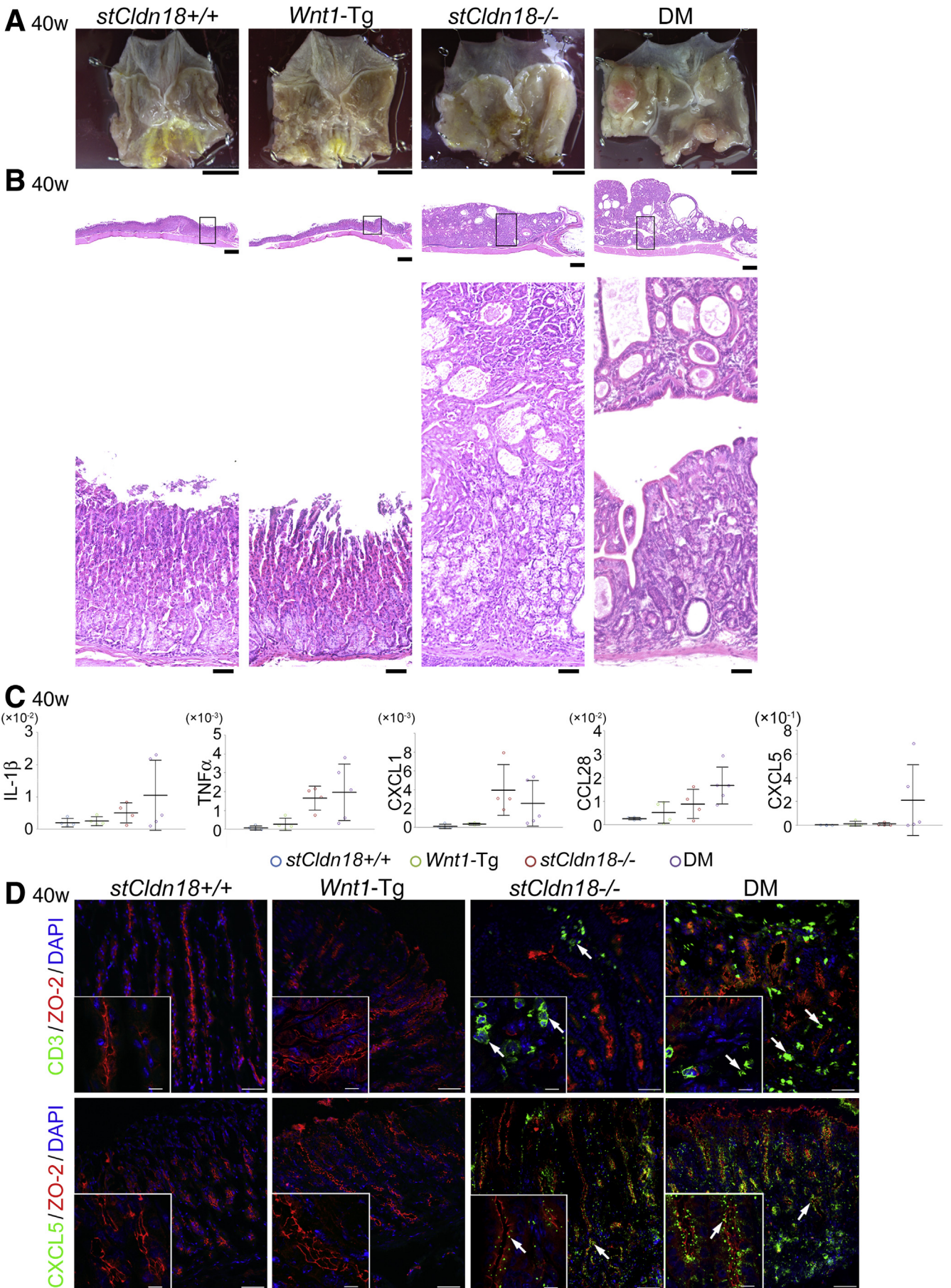
For the immunofluorescent staining of paraffin sections, deparaffinized and hydrated 5-$\mu$m-thick sections were prepared as described above. The samples then underwent antigen retrieval in deionized distilled water containing 0.5% Immunosaver (Nissin EM, Tokyo, Japan) at 98°C for 45 minutes. After antigen retrieval, the samples were washed 3 times with PBS. The samples were then blocked, and stained with appropriate antibodies as described above.

## Microscopy

Immunofluorescent images were captured or tiled by an LSM710 confocal laser-scanning microscope (Carl Zeiss Japan, Tokyo, Japan) equipped with a 405-nm blue diode laser, 488-nm argon laser, 561-nm DPSS laser, and 633-nm HeNe laser, and with a Plan-Apochromat 20×/0.8 M27 objective, C-Apochromat 40×/1.2 W Corr M27 objective, and C-Apochromat 63×/1.20 W Corr M27 objective. The acquired images were analyzed by ZEN 2012 (Carl Zeiss Japan).

Bright field images were captured or tiled by a BZ-X700 all-in-1 microscope (Keyence Japan, Osaka, Japan) equipped with CFI Plan Apo λ4x, CFI Plan Apo λ10x, CFI Plan Apo λ20x, and CFI Plan Apo λ40x objectives. The acquired images were analyzed by a BZ-X Analyzer (Keyence Japan).

## Flow Cytometry

A glandular portion of a freshly excised mouse stomach was washed with cold PBS, and minced with scissors. The minced tissue was washed twice with cold PBS and centrifuged at 600 $g$ at 4°C for 5 minutes, then incubated in 20 mL of Hank's balanced salt solution (HBSS) containing 10% fetal bovine serum (FBS), 50-mM EDTA, and 15-mg/mL dithiothreitol at 37°C for 10 minutes. After centrifugation at 600 $g$ at room temperature for 10 minutes, the tissue was resuspended and incubated in HBSS containing 300 U/mL collagenase type 1 (Worthington Biochemical Corporation, Lakewood, NJ; Cat. No. LS004196), 0.01/mg/mL DNase 1 (Roche Diagnostics, Tokyo, Japan; Cat. No. 10104159001), and 10% FBS at 37°C for 50 minutes with intermittent pipetting. The recovered cells were sequentially filtered using a 100-, 40-, and 10-$\mu$m-pore-sized nylon mesh. After filtration, the single-cell suspension was blocked with HBSS containing 1% FBS (FBS/HBSS), and stained with fluorescently labeled antibodies at 4°C for 30 minutes. After staining, the cell suspension was washed 3 times with HBSS, each followed by centrifugation at 300 $g$ at 4°C for 5 minutes. The final cell pellet was resuspended in 1% FBS/HBSS containing 1-$\mu$g/mL propidium iodide (Nacalai tesque, Kyoto, Japan; Cat. No. 29037-92). The cell suspension was analyzed using a BD FACSCanto II (BD Biosciences Japan, Tokyo, Japan) and FlowJo software (FlowJo LLC, Ashland, OR).

## Quantitative Real-Time Polymerase Chain Reaction

A freshly excised mouse stomach was cut into small pieces, which were quickly immersed into 500 $\mu$L of RNAlater (Sigma-Aldrich Japan, Tokyo, Japan; Cat. No. R0901-500ML). The stomach tissue was then frozen in liquid $N_2$, fractured using an SK-100 mill (Tokken, Inc, Chiba, Japan), and processed for RNA isolation. The total RNA was isolated using an RNeasy Mini Kit (Qiagen, Tokyo, Japan; Cat. No. 74106), and complementary DNA was synthesized using ReverTraAce (Toyobo, Osaka, Japan; Cat. No. TRT-101) according to the manufacturers' instructions. Quantitative RT-PCR (qRT-PCR) was performed using the QuantiTect SYBR Green PCR Kit (Qiagen; Cat. No. 204143), and the 7900HT Fast Real-Time PCR System (Applied Biosystems Japan, Tokyo, Japan). The oligonucleotide sequences for qRT-PCR are listed in Table 2.

## POL7085 and Cimetidine Administration

POL7085 (Polyphor Ltd, Allschwil, Switzerland) (15 mg/kg body weight/250 $\mu$L in saline containing 0.03% dimethyl sulfoxide, each day), or cimetidine (Nacalai tesque; Cat. No.09031-14) (20 mg/kg body weight/250 $\mu$L in saline containing 0.05% methanol, each day) were intraperitoneally administered to around 50 w.o. mice using a 1-mL syringe (Terumo, Tokyo, Japan; Cat. No. SS-01T) with a 27-gauge needle (Terumo; Cat. No. NN-2719S). Saline containing 0.03% dimethyl sulfoxide or 0.05% methanol was used as the vehicle control. After 1 week of daily administration, the mouse stomach was excised and subjected to qRT-PCR analysis as described above.

---

**Figure 10. (See previous page).** **Accelerated gastric tumorigenesis under chronic active gastritis in aged *Wnt1*-Tg *stCldn18*–/– DM mice.** (*A*) Macroscopic images of the stomach from *stCldn18*+/+, *Wnt1*-Tg, *stCldn18*–/–, and DM mice at middle age (40 w.o.). Gastric tumors were observed in all of the stomachs of DM mice but not of *stCldn18*–/– mice at middle age (40 w.o.). Representative images from at least 3 independent experiments are shown. Scale bars = 1 cm. (*B*) Hematoxylin and eosin–stained images of the stomach from *stCldn18*+/+, *Wnt1*-Tg, *stCldn18*–/–, and DM mice at middle age (40 w.o.). Dysplastic changes were observed in the stomach of DM mice at middle age (40 w.o.). Representative images from at least 2 independent experiments are shown. Scale bars = low magnification = 1 mm, high magnification = 50 $\mu$m. (*C*) Expression levels of IL-1$\beta$, TNF-$\alpha$, CXCL1, CCL28, and CXCL5 in the stomach from s*tCldn18*+/+, *Wnt1*-Tg, *stCldn18*–/–, and DM mice at middle age (40 w.o.) quantified by qRT-PCR (n = 4, 4, 4, 5). The expression levels of IL-1$\beta$, CCL28, and CXCL5 were increased in the stomach of *stCldn18*–/– and DM mice compared with those of *stCldn18*+/+ and *Wnt1*-Tg mice at middle age. Gene expressions were normalized to GAPDH. Results are expressed as mean ± SD. Comparisons among more than 3 groups were performed using the Kruskal-Wallis 1-way ANOVA on ranks ($P < .01$) followed by the Steel-Dwass test. no symbol, not significant. (*D*) Immunofluorescence micrographs for CD3 or CXCL5 (*green*) co-stained with ZO-2 (*red*) and DAPI (*blue*) in the stomach from *stCldn18*+/+, *Wnt1*-Tg, *stCldn18*–/–, and DM mice at middle age (40 w.o.). The levels of CD3- and CXCL5-positive cells (*arrows*) were increased in the stomach of *stCldn18*–/– and DM mice at middle age (40 w.o.). High-magnification images are shown in insets. Representative images from at least 3 independent experiments are shown. Scale bars = 50 $\mu$m, 10 $\mu$m.
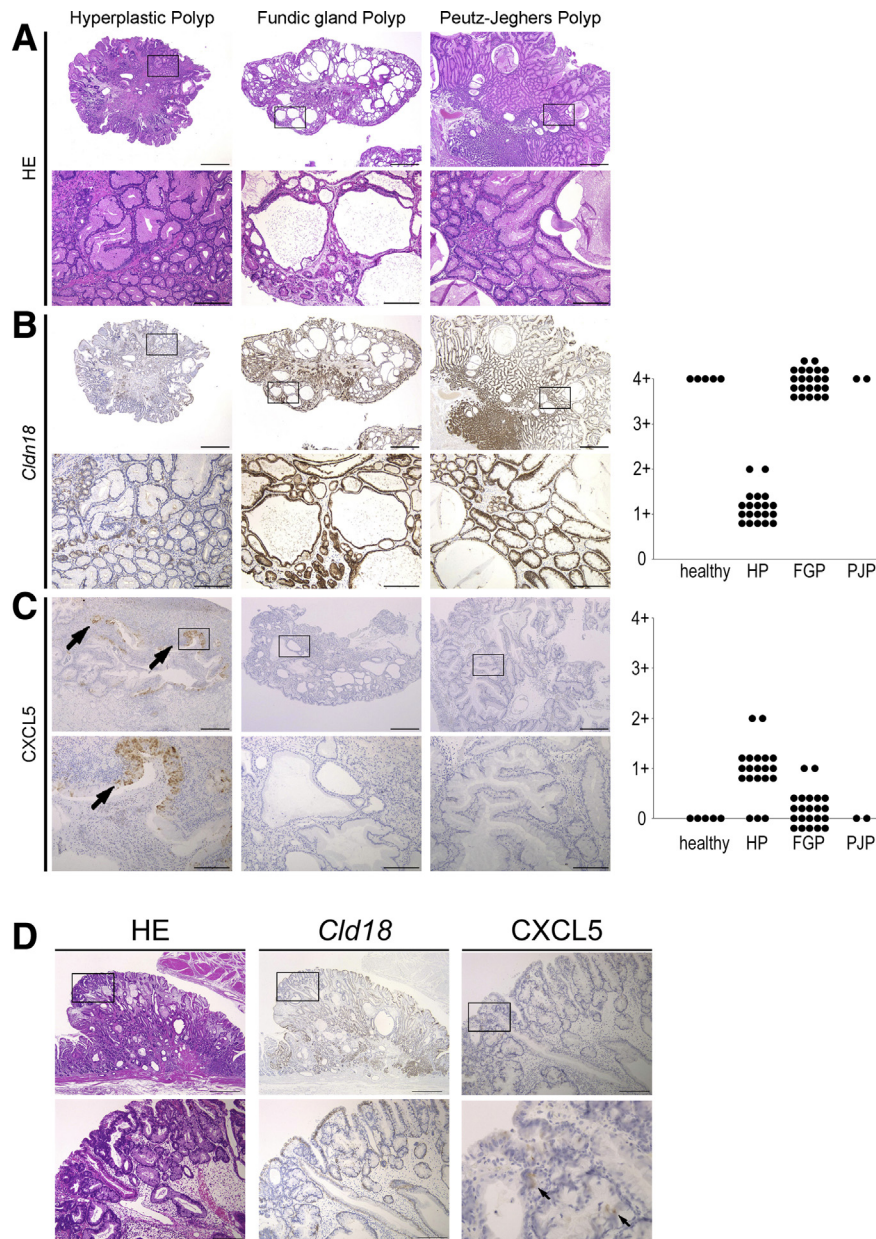
**Figure 11. Inverse correlation between the expression levels of *Cldn18* and CXCL5 in human HP and cancer.** (*A*) Hematoxylin and eosin–stained images of human HP, FGP, and PJP. These gastric tumors are the result of *H pylori* infection, a side effect of proton pump inhibitor therapy, and an inherited gastric tumor of hamartoma/hyperplasia, respectively. Lower panels are magnified images of the boxed regions in the upper panels. Representative images from at least 3 independent experiments are shown. Scale bars = 1 mm and 200 $\mu$m in the upper and lower panels, respectively. (*B*) (*Left*) Immunohistological micrographs for *Cldn18* in human HP, FGP, and PJP. Lower panels are magnified images of the boxed regions in the upper panels. Representative images from at least 3 independent experiments are shown. Scale bars = 1 mm and 200 $\mu$m in the upper and lower panels, respectively. (*Right*) In the graphs, 4+: 75%–100%, 3+: 50%–75%, 2+: 25%–50%, 1+: 1%–25%, 0: 0% of the epithelial cells were stained. The number of Cldn18-positive gastric epithelial cells was significantly decreased in human HP compared with FGP and PJP. (*C*) (*Left*) Immunohistological micrographs for CXCL5 in human HP, FGP, and PJP. Lower panels are magnified images of the boxed regions in the upper panels. Representative images from at least 3 independent experiments are shown. Scale bars = 1 mm and 200 $\mu$m in the upper and lower panels, respectively. (*Right*) In the graphs, 4+: 75%–100%, 3+: 50%–75%, 2+: 25%–50%, 1+: 1%–25%, 0: 0% of the epithelial cells were stained. The number of CXCL5-positive gastric epithelial cells (*arrows*) was significantly increased in human HP compared with FGP and PJP. (*D*) (*Left*) Hematoxylin and eosin–stained images of a human gastric adenoma. Lower panels are magnified images of the boxed regions in the upper panels. Representative images from at least 2 independent experiments are shown. Scale bars = 1 mm and 200$\mu$m in the upper and lower panels, respectively. (*Middle, Right*) Immunohistological micrographs for claudin-18 and CXCL5 in the human gastric adenoma. Lower panels are magnified images of the boxed regions in the upper panels. Representative images from at least 2 independent experiments are shown. Scale bars = 1 mm and 200 $\mu$m in the upper and lower panels, respectively.
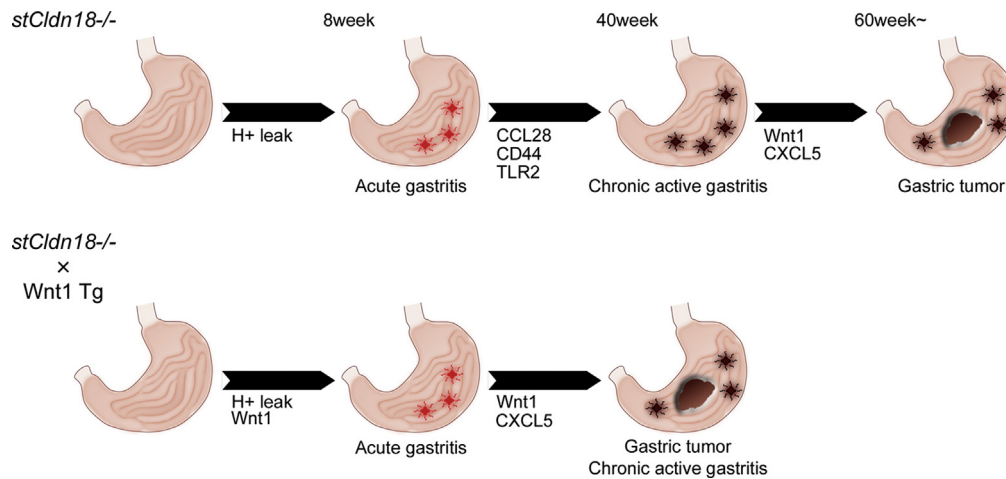
**Figure 12. Schematic illustration of the signaling pathways in *stCldn18–/–* mouse gastric tumorigenesis.** Scheme of the signaling pathways in *stCldn18–/–* mouse gastric tumorigenesis. In the gastric tumorigenesis of *stCldn18–/–* mice, several signaling pathways, including the cytokine-, stemness-, and Wnt- signaling pathways, may be activated to accelerate gastric tumorigenesis under the *stCldn18* deficiency–induced chronic active gastritis.

## Statistical Analysis

All data were expressed as the mean ± SD. Comparisons between 2 groups were performed using Student's *t* test, and differences with *P* < .05 were considered statistically significant. Comparisons among more than 3 groups were performed using the Kruskal-Wallis 1-way analysis of variance on ranks (*P* < .01) followed by the Steel-Dwass test.

**Table 1.** Antibodies Used in Immunofluorescence Images and FACS Analysis

| Epitope | Supplier | Catalog number | Conjugate |
|---|---|---|---|
| Ki-67 | Santa Cruz Biotechnology | sc-7846 | Unconjugate |
| H,K-ATPase | MBL | D031-3 | Unconjugate |
| Gr-1 | BD Pharmingen | 553123 | Unconjugate |
| CD3 | BD Pharmingen | 555273 | Unconjugate |
| CXCL5 | Bioss Antibodies | bs-2549R | Unconjugate |
| CXCL5 | Cell Signaling Technology | MAB433 | Unconjugate |
| CCL28 | BioLegend | 525802 | Unconjugate |
| TFF2 | Bioss Antibodies | bs-1921R | Unconjugate |
| Pepsin C | Santa Cruz Biotechnology | sc-51188 | Unconjugate |
| CD44 | BioLegend | 103001 | Unconjugate |
| TLR2 | BioLegend | 121802 | Unconjugate |
| E-cadherin | Dr. Masatoshi Takeichi | ECCD-2 | Unconjugate |
| $\alpha$-catenin | Sigma | C-2081 | Unconjugate |
| ZO-2 | Santa Cruz Biotechnology | sc-8148 | Unconjugate |
| Claudin-2 | Immuno-Biological Laboratories | 18825 | Unconjugate |
| Claudin-4 | Invitrogen | 364800 | Unconjugate |
| Claudin-7 | Invitrogen | 349100 | Unconjugate |
| Claudin-18 | LifeSpan BioSciences | LS-C146633 | Unconjugate |
| Villin | Santa Cruz Biotechnology | sc-7672 | Unconjugate |
| Active $\beta$-catenin | Cell Signaling Technology | 88145 | Unconjugate |
| CD4 | BioLegend | 100515 | APC |
| CD8a | BioLegend | 100723 | Alexa488 |
| CD11b | BioLegend | 101217 | Alexa488 |
| Ly-6G | BioLegend | 127613 | APC |

**Table 2.** Primer Sequences for Quantitative Real-Time PCR

| Gene | Forward primer | Reverse primer |
|---|---|---|
| *IL-1b* | GCCTCGTGCTGTCGGACC | TGTCGTTGCTTGGTTCTCCTTG |
| *TNF-a* | AGGCTGCCCCGACTACGT | GACTTTCTCCTGGTATGAGATAGCAAA |
| *CXCL1* | TGAGCTGCGCTGTCAGTGCCT | AGAAGCCAGCGTTCACCAGA |
| *CXCL5* | GCATTTCTGTTGCTGTTCACGCTG | CCTCCTTCTGGTTTTTCAGTTTAGC |
| *CCL28* | GAAGCGCATGGAGCTCTGA | AGCTAGGTGGATCTCTGTGAGTTTG |
| *STAT3* | GGATCGCTGAGGTACAACCC | GTCAGGGGTCTCGACTGTCT |
| *NFkB* | GAAATTCCTGATCCAGACAAAAAC | ATCACTTCAATGGCCTCTGTGTAG |
| *IKKb* | TTCCAGCTGAGGAAAGTG TG | AGCTGTTATTCCGGAGGAGA |
| *ASCL2* | GCCTACTCGTCGGAGGAA | CCAACTGGAAAAGTCAAGCA |
| *TLR2* | AACCTCAGACAAAGCGTCAAATC | ACCAAGATCCAGAAGAGCCAAA |
| *c-Myc* | ATGCCCCTCAACGTGAACTTC | CGGAGTCGTAGTCGAGGTCATA |
| *HIF2a* | TGAGTTGGCTCATGAGTTGC | TTGCTGATGTTTTCCGACAG |
| *MMP7* | AGGTGTGGAGTGCCAGATGTTG | CCACTACGATCCGAGGTAAGTC |
| *sox2* | GGCAGCTACAGCATGATGCAGGAGC | CTGGTCATGGAGTTGTACTGCAGG |
| *Wnt1* | AAATGGCAATTCCGAAACC | GAAGATGAACGCTGTTTCTCG |
| *Wnt2* | AAATGGCAATTCCGAAACC | GAGGTGATTGCGAAGATGAA |
| *Wnt3* | AGGAGTGCCAGCATCAGTTC | ACTTCCAGCCTTCTCCAGGT |
| *Wnt4* | CTGGAGAAGTGTGGCTGTGA | CAGCCTCGTTGTTGTGAAGA |
| *Wnt5* | CAAATAGGCAGCCGAGAGAC | CTCTAGCGTCCACGAACTCC |
| *mCldn-1* | CTGGAAGATGATGAGGTGCAGAAGA | CCACTAATGTCGCCAGACCTGAA |
| *mCldn-2* | ATACTACCCTTTAGCCCTGACCGAGA | CAGTAGGAGCACACATAACAGCTACCAC |
| *mCldn-3* | CACCACTACCAGCAGTCGATGAAC | AGACTGTGTGTCGTCTGTCACCATC |
| *mCldn-4* | GGTAGCTCAGCTGTGACTTTGGACTC | CTGGAGTAACGTGTAGGCTGAGTGAG |
| *mCldn-5* | TAACCTGAAAGGGCAGCTGGAGAAAC | AGGTCCAGGCTAAGTCCTTTGGTTCAGTAG |
| *mCldn-6* | TGCCCACTCTATCATCCAGGACTTC | AGGCCTGAGGCTGCCCAG |
| *mCldn-7* | ACGCCCATGAACGTTAAGTACGAG | CTTTGCTTTCACTGCCTGGACA |
| *mCldn-8* | CTGGGGATAAAAGAGAAGGAGGCTGA | AGGCTGCAAAGCAGGATAGCAGAAAG |
| *mCldn-9* | CTTGAGCTAACCCTCTGTAGTGGTTG | CCAGAGTAAGAAAGTCCAGGAGAGCA |
| *mCldn-10.1* | TGGGTGCTAGTGTCTTCCACACTG | GAATCGGTAACGCAGATCTTCCAC |
| *mCldn-10.2* | TCCCACACTTCAAGCCATGAGA | GCAGACACTGGACAAAACTTCCAC |
| *mCldn-11* | CTGCCGAAAAATGGACGAACTG | TGCACGTAGCCTGGAAGGATGA |
| *mCldn-12* | CAGACCAGTGTGTACTCAGACTTTCTACCC | GAAGCAACATACTGACTGTCTCCTGACG |
| *mCldn-13* | GTCAACATCCCAGTATGCAGAGACTTTC | GCTGGCCATCAAACATCTAAGGTATC |
| *mCldn-14* | GCAGCGTTGATAGCTGAAACTAGGTG | CCAAGGCTGCTAGAAACTTTGCTG |
| *mCldn-15* | GCAGGGACCCTCCACATACTTG | AGTTCATACTTGGTTCCAGCATACAGTG |
| *mCldn-16* | CTGGAGGTGAGCACTAAATGCAGAG | AGTTACCACCAGCTTCAAGGGATGTTC |
| *mCldn-17* | CTTCCACCAGCTACGTCTAAGGCTTACTTC | CTGAAGTACTCACAGTTTCTGGGGTGAC |
| *mCldn-18-1.2A* | AGTATGAAGGGCTCTGGAGGAGTTG | AGAACAATGCCCACGATCATCAG |
| *mCldn-18-2.1A* | GTATTCAACTACCAAGGGCTATGGCGTTC | ATCATCAGGGCTCGTACAGCTTGC |
| *mCldn-19* | CAGGTCTCTGTACTTTGACTGCTGTCTC | CCAAATTCGTACCTGGCATTGAC |
| *mCldn-20* | GGTACACCAAGGAGATCATAGCGAAC | ATGTACAGGGCTCCTCCAGGTTCATA |
| *mClaudin21* | CTGGGACTATTGGGACTTCTG | AGGAGACTGGAAAGAGGGTAG |
| *mCldn22* | CTCCCAGAACGTTCTAATGGGCTTAG | AGTGCGGCAAGTAGTTTGTAAGGCAG |
| *mCldn-23* | TGGAGTCTGAGGGTGACTTGAACTTCTG | AAGGAAGGCTTGACCTCCAGTTAGAGGAAG |
| *mClaudin24* | GATCATGGTTCATACCTAG | TAAGGACACGACTCGGC |
| *mClaudin25* | ACGAGCAGTTCATGGAGAAG | CAAAGCACATCAAGCCCAAG |
| *mClaudin26* | ATGAACCCTTTCTGGCAGG | AACACCATCACGATCAGACTG |
| *mClaudin27* | ATCGTATGTGGTTGGGTCTG | GGTGTGAGTAGCTGATGTAGATG |

# References

1. Correia AL, Bissell MJ. The tumor microenvironment is a dominant force in multidrug resistance. Drug Resist Updat 2012;15:39–49.
2. Fidler IJ, Kripke ML. Metastasis results from preexisting variant cells within a malignant tumor. Science 1977; 197:893–895.
3. Joyce JA, Pollard JW. Microenvironmental regulation of metastasis. Nat Rev Cancer 2009;9:239–252.
4. Bhat R, Bissell MJ. Of plasticity and specificity: dialectics of the microenvironment and macroenvironment and the organ phenotype. Wiley Interdiscip Rev Membr Transp Signal 2014;3:147–163.
5. Frank JA. Claudins and alveolar epithelial barrier function in the lung. Ann N Y Acad Sci 2012; 1257:175–183.
6. Abu-Odeh M, Bar-Mag T, Huang H, Kim TH, Salah Z, Abdeen SK, Sudol M, Reichmann D, Sidhu S, Kim PM, Aqeilan RI. Characterizing WW domain interactions of tumor suppressor WWOX reveals its association with multiprotein networks. J Biol Chem 2014;289:8865–8880.
7. Tsukita S, Furuse M, Itoh M. Multifunctional strands in tight junctions. Nat Rev Mol Cell Biol 2001;2:285–293.
8. Shen L. Tight junctions on the move: molecular mechanisms for epithelial barrier regulation. Ann N Y Acad Sci 2012;1258:9–18.
9. Suzuki H, Tani K, Tamura A, Tsukita S, Fujiyoshi Y. Model for the architecture of claudin-based paracellular ion channels through tight junctions. J Mol Biol 2015; 427:291–297.
10. Peek RM Jr, Blaser MJ. Hellicobactor pylori and gastrointestinal tract adenocarcinomas. Nat Rev Cancer 2016;2:387–402.
11. Higashi H, Nakaya A, Tsutstumi R, Yokoyama K, Fujii Y, Ishikawa S, Higuchi M, Takahashi A, Kurashima Y, Teishikata Y, Tanaka S, Azuma T, Hatakeyama M. Helicobacter pylori CagA induces Ras-independent morphogenetic response through SHP-2 recruitment and activation. J Biol Chem 2004;279:17205–17216.
12. Takahashi A, Tsutsumi R, Kikuchi I, Obuse C, Saito Y, Seidi A, Karisch R, Fernandez M, Cho T, Ohnishi N, Rozenblatt-Rosen O, Meyerson M, Neel BG, Hatakeyama M. SHP2 tyrosine phosphatase converts parafibromin/Cdc73 from a tumor suppressor to an oncogenic driver. Mol Cell 2011;43:45–56.
13. Saadat I, Higashi H, Obuse C, Umeda M, Murata-Kamiya N, Saito Y, Lu H, Ohnishi N, Azuma T, Suzuki A, Ohno S, Hatakeyama M. Helicobacter pylori CagA targets PAR1/MARK kinase to disrupt epithelial cell polarity. Nature 2007;447:330–333.
14. Hayashi D, Tamura A, Tanaka H, Yamazaki Y, Watanabe S, Suzuki K, Suzuki K, Sentani K, Yasui W, Rakugi H, Isaka Y, Tsukita S. Deficiency of claudin–18 causes paracellular H+leakage, upregulation of interleukin–1$\beta$, and atrophic gastritis in mice. Gastroenterology 2012;142:292–304.
15. Mineta K, Yamamoto Y, Yamazaki Y, Tanaka H, Tada Y, Saito K, Tamura A, Igarashi M, Endo T, Takeuchi K, Tsukita S. Predicted expansion of the claudin multigene family. FEBS Lett 2011;585:606–612.
16. Tsukita S, Furuse M, Itoh M. Structural and signalling molecules come together at tight junctions. Curr Opin Cell Biol 1999;11:628–633.
17. Tanaka H, Takechi M, Kiyonari H, Shioi G, Tamura A, Tsukita S. Intestinal deletion of claudin-7 enhances paracellular organic solute flux and initiates colonic inflammation in mice. Gut 2015;64:1529–1538.
18. Matsumoto K, Imasato M, Yamazaki Y, Tanaka H, Watanabe M, Eguchi H, Nagano H, Hikita H, Tatsumi T, Takehara T, Tamura A, Tsukita S. Claudin 2 deficiency reduces bile flow and increases susceptibility to cholesterol gallstone disease in mice. Gastroenterology 2014;147:1134–1145.e10.
19. Wada M, Tamura A, Takahashi N, Tsukita S. Loss of claudins 2 and 15 from mice causes defects in paracellular Na+flow and nutrient transport in gut and leads to death from malnutrition. Gastroenterology 2013; 144:369–380.
20. Tamura A, Tsukita S. Paracellular barrier and channel functions of TJ claudins in organizing biological systems: advances in the field of barriology revealed in knockout mice. Semin Cell Dev Biol 2014;36:177–185.
21. Tokumasu R, Yamaga K, Yamazaki Y, Murota H, Suzuki K, Tamura A, Bando K, Furuta Y, Katayama I, Tsukita S. Dose-dependent role of claudin–1 in vivo in orchestrating features of atopic dermatitis. Proc Natl Acad Sci U S A 2016;113:E4061–E4068.
22. Van Itallie CM, Anderson JM. Claudins and epithelial paracellular transport. Annu Rev Physiol 2006; 68:403–429.
23. Guillemot L, Paschoud S, Pulimeno P, Foglia A, Citi S. The cytoplasmic plaque of tight junctions: a scaffolding and signalling center. Biochim Biophys Acta 2008; 1778:601–613.
24. Yao F, Kausalya JP, Sia YY, Teo ASM, Lee WH, Ong AGM, Zhang Z, Tan JHJ, Li G, Bertrand D, Liu X, Poh HM, Guan P, Zhu F, Pathiraja TN, Ariyaratne PN, Rao J, Woo XY, Cai S, Mulawadi FH, Poh WT, Veeravalli L, Chan CS, Lim SS, Leong ST, Neo SC, Choi PS, Chew EG, Nagarajan N, Jacques PE, So JB, Ruan X, Yeoh KG, Tan P, Sung WK, Hunziker W, Ruan Y, Hillmer AM. Recurrent fusion genes in gastric cancer: CLDN18-ARHGAP26 induces loss of epithelial integrity. Cell Rep 2015;12:272–285.
25. Tsukita S, Tanaka H, Tamura A. The claudins: from tight junctions to biological systems. Trends Biochem Sci 2019;44:141–152.
26. Multhoff G, Molls M, Radons J. Chronic inflammation in cancer development. Front Immunol 2012;2:1–17.
27. Hagen SJ, Ang L-H, Zheng Y, Karahan SN, Wu J, Wang YE, Caron TJ, Gad AP, Muthupalani S, Fox JG. Loss of tight junction protein Claudin 18 promotes progressive neoplasia development in mouse stomach. Gastroenterology 2018:1–16.
28. Zhang XY, Zhang PY, Aboul-Soud MAM. From inflammation to gastric cancer: role of Helicobacter pylori. Oncol Lett 2017;13:543–548.
29. Nakagawa H, Umemura A, Taniguchi K, Font-Burgada J, Dhar D, Ogata H, Zhong Z, Valasek MA, Seki E, Hidalgo J, Koike K, Kaufman RJ, Karin M. ER stress

cooperates with hypernutrition to trigger TNF-dependent spontaneous HCC development. Cancer Cell 2014; 26:331–343.

30. Katoh H, Wang D, Daikoku T, Sun H, Dey SK, DuBois RN. CXCR2-expressing myeloid-derived suppressor cells are essential to promote colitis-associated tumorigenesis. Cancer Cell 2013;24:631–644.

31. Takahashi E, Nagano O, Ishimoto T, Yae T, Suzuki Y, Shinoda T, Nakamura S, Niwa S, Ikeda S, Koga H, Tanihara H, Saya H. Tumor necrosis factor-?? regulates transforming growth factor-??-dependent epithelial-mesenchymal transition by promoting hyaluronan-CD44-moesin interaction. J Biol Chem 2010; 285:4060–4073.

32. Yamanoi K, Arai E, Tian Y, Takahashi Y, Miyata S, Sasaki H, Chiwaki F, Ichikawa H, Sakamoto H, Kushima R, Katai H, Yoshida T, Sakamoto M, Kanai Y. Epigenetic clustering of gastric carcinomas based on dna methylation profiles at the precancerous stage: Its correlation with tumor aggressiveness and patient outcome. Carcinogenesis 2015;36:509–520.

33. Lamouille S, Xu J, Derynck R. Molecular mechanisms of epithelial-mesenchymal transition. Nat Rev Mol Cell Biol 2014;15:178–196.

34. Zhou SL, Zhou ZJ, Hu ZQ, Li X, Huang XW, Wang Z, Fan J, Dai Z, Zhou J. CXCR2/CXCL5 axis contributes to epithelial-mesenchymal transition of HCC cells through activating PI3K/Akt/GSK-3$\beta$/Snail signaling. Cancer Lett 2015;358:124–135.

35. Ohata H, Kitauchi S, Yoshimura N, Mugitani K, Iwane M, Nakamura H, Yoshikawa A, Yanaoka K, Arii K, Tamai H, Shimizu Y, Takeshita T, Mohara O, Ichinose M. Progression of chronic atrophic gastritis associated with Helicobacter pylori infection increases risk of gastric cancer. Int J Cancer 2004;109:138–143.

36. Tye H, Kennedy CL, Najdovska M, McLeod L, McCormack W, Hughes N, Dev A, Sievert W, Ooi CH, Ishikawa TO, Oshima H, Bhathal PS, Parker AE, Oshima M, Tan P, Jenkins BJ. STAT3-driven upregulation of TLR2 promotes gastric tumorigenesis independent of tumor inflammation. Cancer Cell 2012; 22:466–478.

37. Bromberg J, Wang TC. Inflammation and cancer: IL-6 and STAT3 complete the Link. Cancer Cell 2009; 15:79–80.

38. Groisman GM, Depsames R, Ovadia B, Meir A. Metastatic carcinoma occurring in a gastric hyperplastic polyp mimicking primary gastric cancer: the first reported case. Case Rep Pathol 2014;2014:1–5.

39. Barham W, Chen L, Tikhomirov O, Onishko H, Gleaves L, Stricker TP, Blackwell TS, Yull FE. Aberrant activation of NF-$\kappa$B signaling in mammary epithelium leads to abnormal growth and ductal carcinoma in situ. BMC Cancer 2015;15:1–17.

40. Hansson M, Hermansson M, Svensson H, Elfvin A, Hansson LE, Johnsson E, Sjöling Å, Quiding-Järbrink M. CCL28 is increased in human Helicobacter pylori-induced gastritis and mediates recruitment of gastric immunoglobulin A-secreting cells. Infect Immun 2008; 76:3304–3311.

41. Thomas MA, Buelow BJ, Nevins AM, Jones SE, Peterson FC, Gundry RL, Grayson MH, Volkman BF. Structure-function analysis of CCL28 in the development of post-viral asthma. J Biol Chem 2015; 290:4528–4536.

42. Facciabene A, Peng X, Hagemann IS, Balint K, Barchetti A, Wang LP, Gimotty PA, Gilks CB, Lal P, Zhang L, Coukos G. Tumour hypoxia promotes tolerance and angiogenesis via CCL28 and Tregcells. Nature 2011; 475:226–230.

43. Huaman MA, Fiske CT, Jones TF, Warkentin J, Shepherd BE, Maruri F, Sterling TR. CCL28 chemokine: An anchoring point bridging innate and adaptive immunity. Int Immunopharmacol 2015;143:951–959.

44. Daubeuf F, Jung F, Douglas GJ, Chevalier E, Frossard N. Protective effect of a protein epitope mimetic CCR10 antagonist, POL7085, in a model of allergic eosinophilic airway inflammation. Respir Res 2015;16:1–11.

45. Buelow BJ, Rohlfing M, Jung F, Douglas GJ, Grayson MH. POL7085 or anti-CCL28 treatment inhibits development of post-paramyxoviral airway disease. Immun Inflamm Dis 2017;5:98–108.

46. Zavros Y. Initiation and maintenance of gastric cancer: a focus on CD44 variant isoforms and cancer stem cells. Cell Mol Gastroenterol Hepatol 2017;4:55–63.

47. Li H, Jasper H. Gastrointestinal stem cells in health and disease: from flies to humans. Dis Model Mech 2016; 9:487–499.

48. Seishima R, Wada T, Tsuchihashi K, Okazaki S, Yoshikawa M, Oshima H, Oshima M, Sato T, Hasegawa H, Kitagawa Y, Goldenring JR, Saya H, Nagano O. Ink4a/arf-dependent loss of parietal cells induced by oxidative stress promotes CD44-dependent gastric tumorigenesis. Cancer Prev Res (Phila) 2015;8:492–501.

49. Wada T, Ishimoto T, Seishima R, Tsuchihashi K, Yoshikawa M, Oshima H, Oshima M, Masuko T, Wright NA, Furuhashi S, Hirashima K, Baba H, Kitagawa Y, Saya H, Nagano O. Functional role of CD44v-xCT system in the development of spasmolytic polypeptide–expressing metaplasia. Cancer Sci 2013;104:1323–1329.

50. Echizen K, Hirose O, Maeda Y, Oshima M. Inflammation in gastric cancer: Interplay of the COX-2/prostaglandin E2and Toll-like receptor/MyD88 pathways. Cancer Sci 2016;107:391–397.

51. Schuijers J, Junker JP, Mokry M, Hatzis P, Koo BK, Sasselli V, Van Der Flier LG, Cuppen E, Van Oudenaarden A, Clevers H. Ascl2 acts as an R-spondin/wnt-responsive switch to control stemness in intestinal crypts. Cell Stem Cell 2015;16:158–170.

52. Weis VG, Goldenring JR. Current understanding of SPEM and its standing in the preneoplastic process. Gastric Cancer 2009;12:189–197.

53. Holmes JL, Van Itallie CM, Rasmussen JE, Anderson JM. Claudin profiling in the mouse during postnatal intestinal development and along the gastrointestinal tract reveals complex expression patterns. Gene Expr Patterns 2006; 6:581–588.

54. Petersen CP, Mills JC, Goldenring JR. Murine models of gastric corpus preneoplasia. Cell Mol Gastroenterol Hepatol 2017;3:11–26.

55. Shimizu T, Choi E, Petersen CP, Noto JM, Romero-Gallo J, Piazuelo MB, Washington MK, Peek RM, Goldenring JR. Characterization of progressive metaplasia in the gastric corpus mucosa of Mongolian gerbils infected with Helicobacter pylori. J Pathol 2016;239:399–410.

56. Chiurillo MA. Role of the Wnt/$\beta$-catenin pathway in gastric cancer: an in-depth literature review. World J Exp Med 2015;5:84–102.

57. Mao J, Fan S, Ma W, Fan P, Wang B, Zhang J, Wang H, Tang B, Zhang Q, Yu X, Wang L, Song B, Li L. Roles of Wnt/$\beta$-catenin signaling in the gastric cancer stem cells proliferation and salinomycin treatment. Cell Death Dis 2014;5:1–9.

58. Brabletz T, Jung A, Dag S, Hlubek F, Kirchner T. B-catenin regulates the expression of the matrix metalloproteinase-7 in human colorectal cancer. Am J Pathol 1999;155:1033–1038.

59. Zhao J, Ou B, Han D, Wang P, Zong Y, Zhu C, Liu D, Zheng M, Sun J, Feng H, Lu A. Tumor-derived CXCL5 promotes human colorectal cancer metastasis through activation of the ERK/Elk-1/Snail and AKT/GSK3$\beta$/$\beta$-catenin pathways. Mol Cancer 2017;16:1–15.

60. Valkenburg KC, Graveel CR, Zylstra-Diegel CR, Zhong Z, Williams BO. Wnt/$\beta$-catenin signaling in normal and cancer stem cells. Cancers 2011;3:2050–2079.

61. Oshima H, Matsunaga A, Fujimura T, Tsukamoto T, Taketo MM, Oshima M. Carcinogenesis in mouse stomach by simultaneous activation of the Wnt signaling and prostaglandin E2 pathway. Gastroenterology 2006; 131:1086–1095.

62. Markowski AR, Markowska A, Guzinska-Ustymowicz K. Pathophysiological and clinical aspects of gastric hyperplastic polyps. World J Gastroenterol 2016; 22:8883–8891.

63. Velázquez-Dohorn ME, López-Durand CF, Gamboa-Domínguez A. Changing trends in gastric polyps. Rev Invest Clin 2018;70:40–45.

64. Kopacova M, Tacheci I, Rejchrt S, Bures J. Peutz-Jeghers syndrome: diagnostic and therapeutic approach. World J Gastroenterol 2009;15:5397–5408.

65. Phesse TJ, Sansom OJ. Lgr5 joins the club of gastric stem cell markers in the corpus. Nat Cell Biol 2017; 19:752–754.

66. Leushacke M, Tan SH, Wong A, Swathi Y, Hajamohideen A, Tan LT, Goh J, Wong E, Denil SLIJ, Murakami K, Barker N. Lgr5-expressing chief cells drive epithelial regeneration and cancer in the oxyntic stomach. Nat Cell Biol 2017;19:774–786.

67. Kinoshita H, Hayakawa Y, Koike K. Metaplasia in the stomach—precursor of gastric Cancer? Int J Mol Sci 2017;18:E2063.

68. Mittal V. Epithelial mesenchymal transition in tumor metastasis. Annu Rev Pathol 2018;13:395–412.

69. Demitrack ES, Samuelson LC. Notch as a driver of gastric epithelial cell proliferation. Cell Mol Gastroenterol Hepatol 2017;3:323–330.

70. Zhou B, Crandall ED, Borok Z, Zhou B, Flodby P, Luo J, Castillo DR, Liu Y, Yu F, Mcconnell A, Varghese B. Claudin-18 – mediated YAP activity regulates lung stem and progenitor cell homeostasis and tumorigenesis Find the latest version: Claudin-18 – mediated YAP activity regulates lung stem and progenitor cell homeostasis and tumorigenesis. J Clin Invest 2018;128:970–984.

**Correspondence**
Address requests for reprints to: Atsushi Tamura, Laboratory of Biological Science, Graduate School of Frontier Biosciences, Osaka University, 2-2Yamadaoka, Suita, Osaka 565-0871, Japan. e-mail: atamura@biosci.med.osaka-u.ac.jp; fax: +81-6-6879-3329, or Sachiko Tsukita, Laboratory of Biological Science, Graduate School of Frontier Biosciences, Osaka University, 2-2 Yamadaoka, Suita, Osaka 565-0871, Japan. e-mail: atsukita@biosci.med.osaka-u.ac.jp; fax: +81-6-6879-3329, or Koya Suzuki, Research Institute for Diseases of Old Age and Department of Clinical Laboratory Medicine, Graduate School of Medicine, Juntendo University, Tokyo, Japan. e-mail: koya-suzuki@juntendo.ac.jp; fax: +81-3-5684-1609.